Molecular Therapy
Methods & Clinical Development
Original Article

Efficient Gene Transfer to the Central Nervous System by Single-Stranded Anc80L65

Eloise Hudry,[1] Eva Andres-Mateos,[2,3] Eli P. Lerner,[1] Adrienn Volak,[4] Olivia Cohen,[1] Bradley T. Hyman,[1] Casey A. Maguire,[4] and Luk H. Vandenberghe[2,3,5,6]

[1]MassGeneral Institute for Neurodegenerative Disease, Massachusetts General Hospital and Harvard Medical School, Charlestown, MA 02129, USA; [2]Grousbeck Gene Therapy Center, Schepens Eye Research Institute and Massachusetts Eye and Ear Infirmary, Boston, MA 02114, USA; [3]Ocular Genomics Institute, Department of Ophthalmology, Harvard Medical School, Boston, MA 02114, USA; [4]Department of Neurology, The Massachusetts General Hospital and NeuroDiscovery Center, Harvard Medical School, Boston, MA 02114, USA; [5]Harvard Stem Cell Institute, Harvard University, Cambridge, MA 02138, USA; [6]The Broad Institute of Harvard and MIT, Cambridge, MA 02142, USA

Adeno-associated viral vectors (AAVs) have demonstrated potential in applications for neurologic disorders, and the discovery that some AAVs can cross the blood-brain barrier (BBB) after intravenous injection has further expanded these opportunities for non-invasive brain delivery. Anc80L65, a novel AAV capsid designed from *in silico* reconstruction of the viral evolutionary lineage, has previously demonstrated robust transduction capabilities after local delivery in various tissues such as liver, retina, or cochlea, compared with conventional AAVs. Here, we compared the transduction efficacy of Anc80L65 with conventional AAV9 in the CNS after intravenous, intracerebroventricular (i.c.v.), or intraparenchymal injections. Anc80L65 was more potent at targeting the brain and spinal cord after intravenous injection than AAV9, and mostly transduced astrocytes and a wide range of neuronal subpopulations. Although the efficacy of Anc80L65 and AAV9 is similar after direct intraparenchymal injection in the striatum, Anc80L65's diffusion throughout the CNS was more extensive than AAV9 after i.c.v. infusion, leading to widespread *EGFP* expression in the cerebellum. These findings demonstrate that Anc80L65 is a highly efficient gene transfer vector for the murine CNS. Systemic injection of Anc80L65 leads to notable expression in the CNS that does not rely on a self-complementary genome. These data warrant further testing in larger animal models.

INTRODUCTION

Adeno-associated viral vectors (AAVs) are considered a vector of choice for *in vivo* gene transfer for various tissues based on an overall attractive safety profile preclinically and clinically. Indeed, AAV is not directly associated with any disease, minimally pro-inflammatory, demonstrates promiscuous tropism for many therapeutic cell and tissue targets, and its genome is stably maintained episomally yet transcriptionally active in the cell nucleus in non-dividing cells.[1–4] These properties have contributed to demonstrations of long-lasting steady-state expression (up to 10 years at least in humans[5]). Data from animal models have shown that AAV can lead to significant therapeutic benefit in inherited,[6–8] acquired,[9–13] and even infectious[14–17] diseases. Excitingly, encouraging results have also been reported in a handful of early-stage clinical trials (phase I/II), such as a dramatically reduced need for protein prophylaxis in hemophilia A and B,[18–20] and remarkable impact on lifespan, motor function, and overall disease in the most severe form of spinal muscular atrophy.[21,22] In January 2018, the first AAV product, voretigene neparvovec, was approved by the Food and Drug Administration (FDA) for the treatment of a form of inherited retinal degeneration.[23]

The ability of AAVs to transduce post-mitotic cells and their strong neuronal tropism has naturally promoted their use in the field of neurosciences, not only for therapeutic purposes, but also as experimental tools to express genetically encoded reporters to interrogate the basic mechanisms underlying neuronal function or brain connectivity.[24–31] In most cases, direct intraparenchymal injection allows to bypass the blood-brain barrier (BBB) and precisely manipulate gene expression with time and spatial resolution, a strategy that has been associated with clinical improvement in many pathological contexts, ranging from neurodevelopmental[32–35] diseases to psychiatric[36,37] or age-related neurodegenerative disorders.[1,38–42] Interestingly, the recent characterization of AAV serotypes able to transduce the CNS after a single intravenous injection in adult mice now offers a non-invasive vector delivery route for the entire neural tissue and the possibility to evaluate the impact of therapeutic candidates for multi-focal neurological disorders.[43–47] Although this approach constitutes a breakthrough for the field, several issues remain when AAV is administered

Received 23 December 2017; accepted 10 July 2018;
https://doi.org/10.1016/j.omtm.2018.07.006.

Correspondence: Luk H. Vandenberghe, PhD, Grousbeck Gene Therapy Center, Schepens Eye Research Institute and Massachusetts Eye and Ear Infirmary, 20 Staniford Street, Boston, MA 02114, USA.
E-mail: luk_vandenberghe@meei.harvard.edu

peripherally for clinical or basic research applications: first, efficient CNS transduction in preclinical models is often conditional to the use of a self-complementary (sc) genome (e.g., AAV9), which greatly limits the insert capacity of the vector (<2.3 kb as opposed to 4.7 kb for single-stranded AAV);[47–51] second, the presence of AAV neutralizing antibodies in human populations where natural AAV infections occur in 30%–90% of individuals can dramatically inhibit the efficacy of gene transfer by systemic delivery;[48,52] and third, ectopic expression of the transgene in peripheral tissues may lead to unwanted side effects (a problem that can be limited by using neural cell-type-specific promoters[53,54]). To overcome those issues, developing novel AAVs that will retain their potential for crossing the BBB, lead to sustained transgene expression from a single-stranded genome, and limit pre-existing immunity is required.

In the present study, we characterized the efficacy and transduction profile of Anc80L65 harboring a single-stranded genome in the CNS, thus preserving the full DNA insert capacity of the vector. As opposed to other AAVs, this relatively novel vector system was designed *in silico* based on ancestral sequence reconstruction with sequence information from natural AAVs, with the primary goal to develop a stable and functional AAV variant, yet serologically and immunologically very distinct from AAVs currently circulating in humans.[55] Anc80L65 had not previously been characterized for CNS targeting, yet has shown remarkable transduction in the anterior segment of the eye,[56] retina,[56,57] and cochlea[58–60] following local injections. We therefore wanted to evaluate Anc80L65 in its ability to target CNS after intravenous, intraparenchymal, and intracerebroventricular routes of delivery. Combining two different reporter approaches by bioluminescence (Firefly luciferase [FLuc]) or fluorescence (EGFP), we demonstrated that a single injection of Anc80L65 into the lateral tail vein of adult immunocompetent mice led to sustained transduction of the entire CNS. Importantly, Anc80L65 largely outperformed the capabilities of AAV9 to target the nervous system and increased the percentage of transduced neurons and astrocytes by a factor 3 and 4.3, respectively. Although this performance remained lower when compared with peripherally delivered AAV9 carrying an sc genome (scAAV9, which is the current configuration used in current clinical trials), the increased transduction capabilities of Anc80L65 will offer novel opportunities to expand the repertoire of therapeutic genes evaluated after systemic delivery. When delivered directly into the brain parenchyma (striatum) or in the lateral cerebral ventricle, less pronounced differences were observed between Anc80L65 and AAV9, even though Anc80L65 further spreads after intracerebroventricular (i.c.v.) injection. Considering the efficient expression of reporter genes in neurons and astrocytes in mice after systemic administration of Anc80L65 carrying a single-stranded genome, this vector is a useful tool for delivery of transgenes in the CNS without the need for packaging an sc genome (which restricts the cloning capacity of the vector by half). These encouraging findings warrant further study of Anc80L65 in larger animal models to evaluate it as a potential candidate for clinical applications.

RESULTS

Bioluminescence Imaging Reveals Higher Signal of Head Region of Mice Systemically Injected with Anc80L65 Encoding FLuc Compared with AAV9-FLuc Vector

To analyze the biodistribution and bodywide transduction pattern of peripherally delivered Anc80L65, we injected in a pilot study BALB/c female mice (n = 5, age 6–8 weeks) via the tail vein with 2×10^{12} genome copies (gc)/kg (5×10^{10} gc/25 g mouse) of Anc80L65 encoding FLuc driven by the cytomegalovirus (CMV) promoter (described in detail in the Materials and Methods). This combination of promoter and transgene allowed for a versatile and highly sensitive evaluation of expression at a moderate dose of vector delivered systemically. For comparison, AAV9 vector carrying the same transgene expression cassette was injected into a separate group of mice (n = 5). Mice were imaged for FLuc-mediated bioluminescence after D-luciferin substrate injection on days 3, 7, 21, and 42 after vector injection (Figures S1 and S2). We observed a remarkably high signal emanating from the liver region at day 3 post-injection in the Anc80L65 group, which was on average 123-fold higher than the AAV9 group at this time point. Signal declined slightly for the Anc80L65 group at day 7 and stabilized for the remaining time points. In contrast, bioluminescent signal from AAV9-FLuc-injected mice increased by 3.7-fold between days 3 and 7 before stabilizing for the remainder of the examined time points (Figure S1A). Interestingly, we also observed a robust bioluminescent signal in the head region of Anc80L65-injected mice (Figure S1B). At day 3, Anc80L65-FLuc-injected mice had an 8.3-fold higher signal from the head region than AAV9-FLuc-injected mice. This enhancement peaked at day 21 with a 34-fold higher signal in the Anc80L65 groups over the AAV9 group. Both groups had an overall slow increase in bioluminescence from days 3 to 42. The bioluminescence data from this pilot study suggested that Anc80L65 might transduce the brain after intravenous (i.v.) delivery; a subsequent study was therefore designed to determine cell-specific transduction properties in the CNS using AAVs that encoded a fluorescent reporter, EGFP, and based on the literature and prior experience, injected at a higher dose in order to obtain sufficient sensitivity to determine cell-intrinsic expression.

Anc80L65 Broadly Transduces the CNS after Systemic Infusion, and Mostly Targets Neurons and Astrocytes in the Brain

In order to get a better understanding of the transduction properties of Anc80L65 in the CNS at a cellular level, another cohort of animals was injected in the lateral tail vein with a vector encoding the EGFP reporter. Due to the relative lack of sensitivity of immunostaining compared with bioluminescence imaging, we infused a higher dose of 4×10^{13} gc/kg (1×10^{12} gc for a 25-g mouse) of Anc80L65-CMV-EGFP and AAV9-CMV-EGFP. We also included a group of mice injected with sc AAV9 (scAAV9) at equal dose as a positive control benchmark because scAAV9 is the current vector of choice used for peripheral approaches in clinical trials[22] and has been previously reported to show a much higher transgene expression as opposed to single-stranded AAV9 via this delivery route.[61,62] The design of the sc and single-stranded (ss) transgene cassettes was

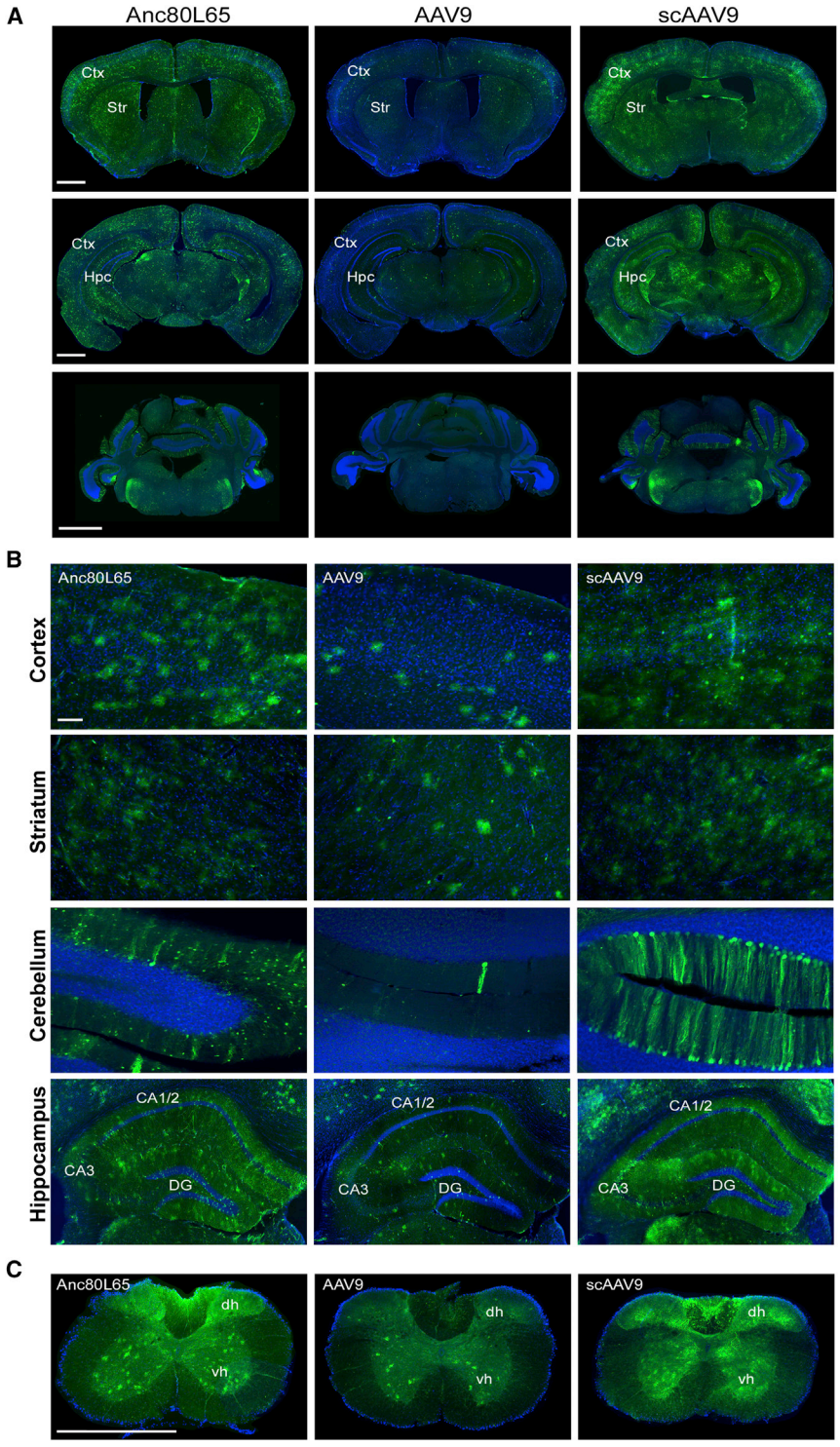

Figure 1. Anc80L65, AAV9, and scAAV9 Transduction Profiles in the CNS after Intravenous Injection

(A) Representative images of EGFP fluorescence signal (and DAPI) across three different coronal sections across the brain: at the level of the striatum (upper panels), hippocampus (middle panels), or cerebellum (bottom panels) after intravenous injection of the same dose of Anc80L65, AAV9, and scAAV9 harboring a self-complementary genome in wild-type mice (4×10^{13} gc/kg). Scale bars: 1,000 μm. (B) A closer view of each section reveals numerous EGFP-positive cells in the cortex (ctx), striatum (str), cerebellum, and hippocampus (hpc) after Anc80L65 infusion. The overall distribution of transduced cells was similar for both AAV9 and scAAV9. Scale bar: 100 μm. (C) Within the spinal cord, AAV transduced cells could be observed in the ventral (vh) and dorsal (dh) horns as well. Scale bar: 500 μm.

made identical to allow for comparability (Figure S6). The number of cells with EGFP signal after Anc80L65 i.v. injection was strikingly higher than AAV9 (lowest EGFP signal), yet lower than scAAV9 (highest EGFP signal), and spread across the entire cerebral tissue (Figure 1A). Cortex, striatum, hippocampus, and cerebellum were homogeneously transduced (Figure 1B), and the distribution of EGFP-positive cells was not significantly different between each vector, even though their overall density varied. Anc80L65 also led to transduction in the spinal cord, again with an intermediate level between single-stranded and sc AAV9 (Figure 1C). These data confirmed our previous observations using the Luciferase reporter system and demonstrated that Anc80L65 can efficiently cross the BBB after peripheral delivery and target the neural tissue. To evaluate the biodistribution of Anc80L65, AAV9, and scAAV9 in peripheral organs after systemic delivery, we determined the number of AAV gc by qPCR in liver, heart, quadriceps, and diaphragm. Anc80L65 led to an intermediate level of vector gc as compared with single-stranded (lowest level of gc/diploid cell) and sc (highest level of gc/diploid cell) AAV9 (Figure S3). Those results suggest that, even though Anc80L65 generally showed a better transduction efficacy as opposed to AAV9, the overall biodistribution of both vectors is not drastically different (as previously reported in our initial characterization of Anc80L65[55]).

In order to characterize which neural cell types were primarily transduced by each AAV after peripheral delivery, we performed co-immunostaining between EGFP and molecular markers of neurons (neuronal nuclei [NeuN]), astrocytes (glutamine synthetase [GS]), microglia (Iba-1), and oligodendrocytes (Olig2). As shown in Figure 2, astrocytes and neurons were transduced by all three AAVs, with different rates of efficacy. Additionally, intraparenchymal

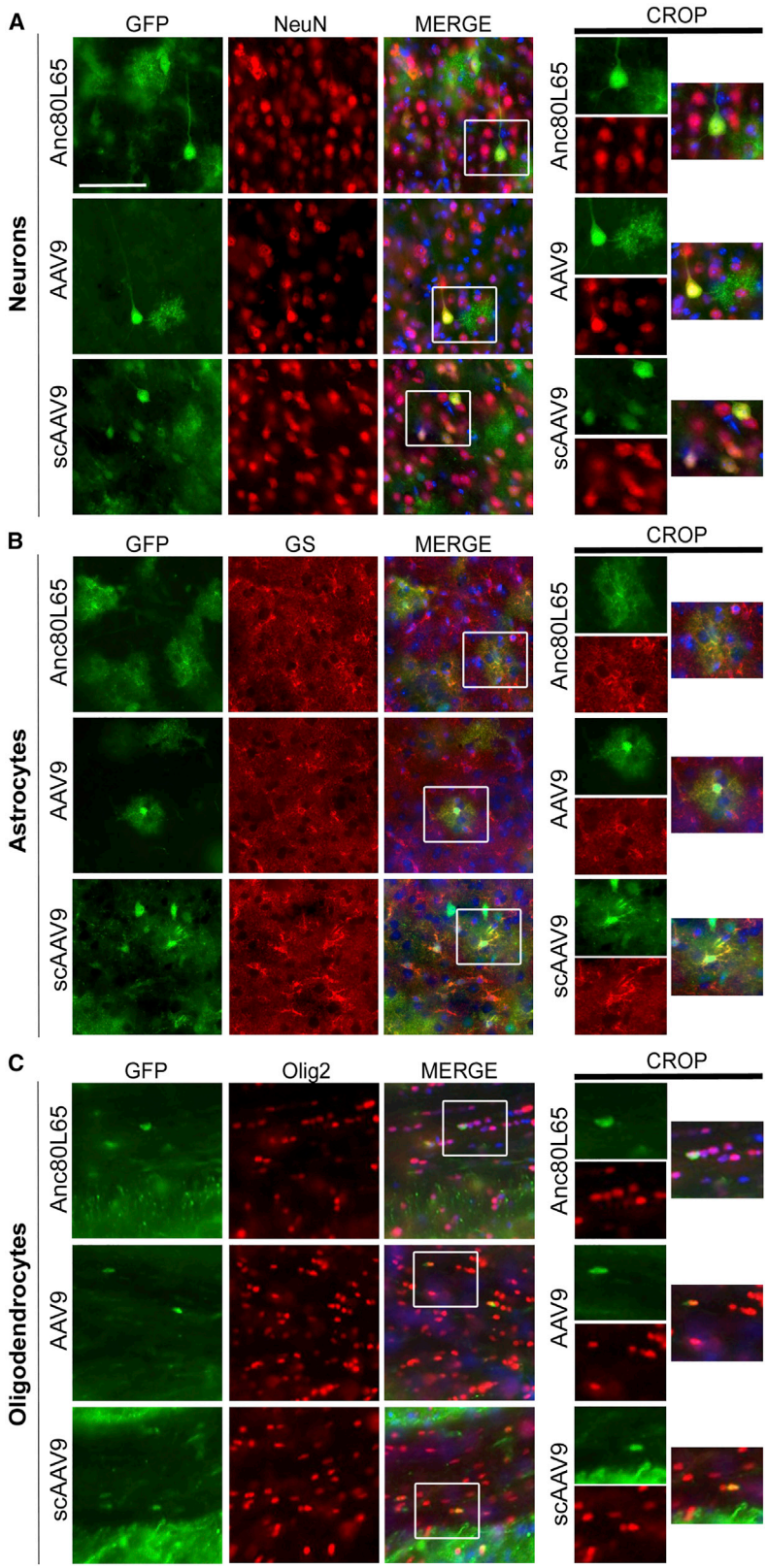

Figure 2. Identification of the Different Neural Cell Types Transduced by Peripherally Administered Anc80L65, AAV9, and scAAV9 Harboring a Self-Complementary Genome

Double immunostainings were performed in order to determine the main neural cell types transduced by each vector. Colocalization between EGFP and NeuN (neuronal nuclei) (A), or EGFP and GS (glutamine synthetase) (B) suggest that neurons and astrocytes are mostly targeted by Anc80L65, AAV9, and scAAV9 delivered intravenously. (C) In the corpus callosum, few oligodendrocytes (identified by the marker Olig2) expressing EGFP were also detected. Higher magnification images of individual cells are presented on the right panels for each cell type. By contrast, no transduced microglial cells (Figure S4) were observed. Scale bar: 50 μm.

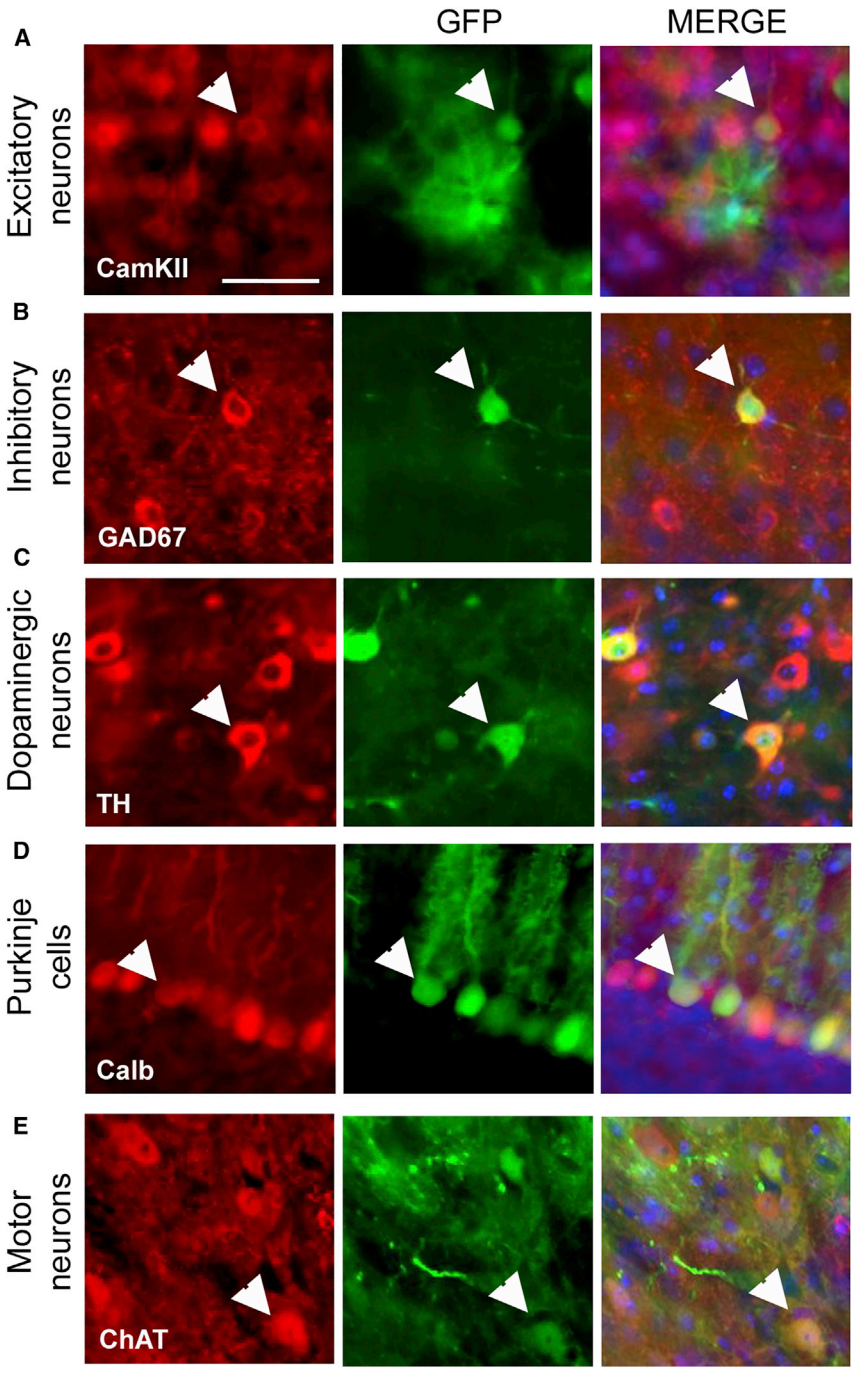

Figure 3. Neuronal Sub-types Targeted by Anc80L65 after Peripheral Injection

Representative images of co-labeling experiments performed to characterize the neuronal sub-types transduced by Anc80L65 (double-positive cells are indicated by white arrows). The colocalization between EGFP with CaMKII (A) or GAD67 (B) markers demonstrates efficient targeting of excitatory and inhibitory neurons, respectively. (C) Interestingly, EGFP/tyrosine hydroxylase (TH)-positive dopaminergic neurons were also observed in the substantia nigra. (D) In the cerebellum, numerous Purkinje cells, identified with the marker Calbindin, express EGFP. (E) In the spinal cord, EGFP-positive motor neurons expressing the choline acetyltransferase (ChAT) were observed. Scale bar: 50 μm.

astrocytes, as well as astrocytic endfeet, were evenly transduced (Figure S4), suggesting that the proximity of astrocytes to blood vessels was not directly correlated with a higher probability of transduction, but that other mechanisms are in play. Seldom EGFP-positive oligodendrocytes were detected, and they were predominantly found in the corpus callosum (Figure 2C). There were virtually no Iba1-positive transduced cells found, indicating that none of the vectors were able to target microglial cells (Figure S5).

To further characterize the neuronal sub-types targeted by Anc80L65-CMV-EGFP after peripheral infusion, we performed additional immunolabeling for specific markers of excitatory neurons (Ca^{2+}/calmodulin-dependent protein kinase II [CaMKII]), inhibitory neurons (glutamate decarboxylase [GAD67]), dopaminergic neurons (tyrosine hydroxylase [TH]), Purkinje cells (calbindin), and motor neurons (choline acetyltransferase [ChAT]), all co-stained for EGFP (Figure 3). In the cortex and hippocampus, a majority of pyramidal excitatory neurons were transduced after i.v. injection of Anc80L65 (Figure 3A), while comparatively fewer inhibitory neurons were detected (Figure 3B). Dopaminergic EGFP-positive neurons in the substantia nigra (Figure 3C), as well as EGFP-positive Purkinje cells in the cerebellum, were numerous (Figure 3D), whereas ChAT/EGFP double-positive cells confirmed that Anc80L65 was also able to target motor neurons (Figure 3E). Overall, those results demonstrate that Anc80L65 efficiently transduces several neuronal sub-types, as well as astrocytes, after systemic injection.

Anc80L65 Transduces Neurons and Astrocytes with a Greater Efficacy Compared with AAV9 after i.v. Delivery When Both Vectors Harbor a Single-Stranded Genome

In order to have a quantitative evaluation of the gene transfer efficacy after i.v. injection of Anc80L65, AAV9, and sc AAV9, we performed in the cortex an unbiased stereological analysis of the percentages of transduced astrocytes and neurons, respectively, identified by the markers GS and NeuN. We quantified the density of EGFP/GS or EGFP/NeuN double-positive cells among the total number of astrocytes or neurons after random sampling of the cortical mantle. We observed that a single injection of Anc80L65 led to the transduction of 6.8% ± 1.3% of neurons and 26.7% ± 5.3% of astrocytes in the cortical mantle, which was significantly higher than AAV9

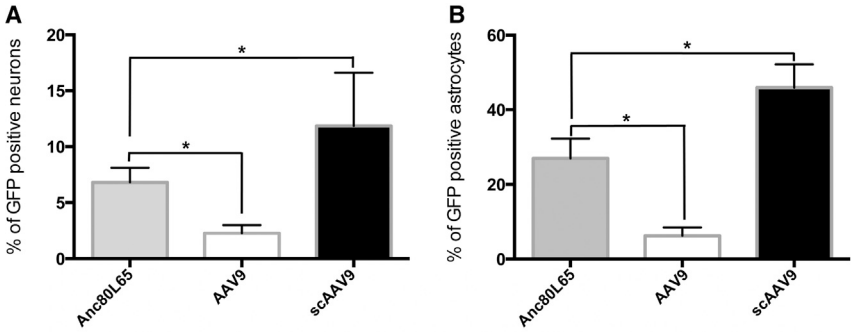

Figure 4. Stereology-Based Quantification of the Percentages of Transduced Neurons and Astrocytes after Peripheral Delivery of Anc80L65, AAV9, and scAAV9 (4×10^{13} gc/kg)

C57BL/6 mice were sacrificed 4 weeks after intravenous injection of Anc80L65, AAV9, or scAAV9. To evaluate the percentage of neuronal transduction, an unbiased stereological analysis of the total number of neurons (identified using the NeuN marker) or astrocytes (identified using the GS marker) and of the total number of NeuN/EGFP and GS/EGFP double-positive cells was achieved by random sampling of the cortex. The percentage of neurons (A) and astrocytes (B) expressing EGFP after transduction by Anc80L65 reached an intermediate level when compared with AAV9 and scAAV9. n = 4 mice per group (two sections analyzed per mouse); non-parametric one-way ANOVA (Kruskal-Wallis test) followed by Dunn's multiple comparison test; *$p < 0.05$. Data are represented as the mean with SD.

(2.3% ± 0.7% and 6.2% ± 2.3%, respectively), but did not reach the levels of sc AAV9 (11.9% ± 4.7% and 45.9% ± 6.2%, respectively; $p < 0.05$, Kruskal-Wallis test followed by a Dunn's multiple comparisons; Figure 4). These results demonstrate that Anc80L65 is advantageous compared with AAV9 when using a single-stranded vector, allowing efficient delivery of transgenes to the CNS after i.v. delivery while preserving the full cloning capacity of AAV.

Direct Intracerebral Injection of Anc80L65 in the Striatum or the Cerebroventricular Space Leads to Widespread Expression of Transgene

While systemic delivery is non-invasive and can lead to transduction of most of the neural tissue at once, targeted intracerebral injections can also offer advantages in certain pathological contexts characterized by focal alteration of the nervous system, achieve clinical efficacy with a much lower dose of vector, and avoid ectopic expression of a specific gene in the periphery. We therefore assessed the performance of Anc80L65 transduction after intrastriatal or intracerebroventricular injections in comparison with conventional AAV9 (both harboring identical single-stranded genomes).

Anc80L65 and AAV9 direct injection profiles in the striatum were rather comparable (Figure 5). Both vectors efficiently transduced the entire region of interest and showed a preferential tropism for neurons as opposed to astrocytes (Figure 5B), in direct contrast with the results observed after i.v. delivery. Injection of Anc80L65 or AAV9 in the lateral ventricle led to more contrasted results (Figure 6), with Anc80L65 showing a higher efficacy at targeting the choroid plexus (Figure 6B) and leading to a much wider transduction pattern as compared with AAV9. In particular, a large number of EGFP-positive Purkinje cells could be detected in the cerebellum, whereas these were seldom detected after AAV9 injection (Figure 6A).

DISCUSSION

Remarkable progress in the field of gene therapy has been made with AAV technologies. Over the past few years, the diversity of the available AAV library has been greatly expanded; initial studies further explored the AAV biodiversity, others modified natural variants rationally, and a third set of strategies that has been a great emphasis of the vector development field has been to leverage methods of library selection via directed evolution.[2,63,64] AAV9 was isolated from a latent viral genome in human tissue by sensitive PCR methods.[65] Anc80L65, on the other hand, was entirely designed *in silico* based on statistical inferences of the putative ancestral sequence state within the primate AAV lineage.[55] Transduction properties in neurosensory targets such as the retina[56] and inner ear[58–60] illustrated its potential for neuronal targeting. Additionally, we observed a low level of cross-reactivity between Anc80L65 and conventional serotypes available, likely because of its significant sequence and structural divergence from the closest AAV sequence rh.10 by 8.6%, an important feature considering that pre-existing immunity against AAV can significantly reduce its efficacy.[66,67]

In order to further characterize this novel variant, the present work specifically studied the transduction capabilities of Anc80L65 in the CNS as compared with AAV9 after i.v., intracerebroventricular, or intrastriatal infusion in adult mice. Of importance, it is conceivable that an sc genome packaged in Anc80L65 would have led to greater performances, because it is the case for conventional AAV9. However, the current study essentially aimed at investigating the transduction capabilities of Anc80L65 based upon the unique characteristics of the capsid of the vector as an ssAAV that preserves the full cloning capacity of AAV, and thereby increases dramatically the number of applications of the technology. In this context, it is important to note that ssAAV genomes at low efficiency are able to package dimeric (analogous to sc) genomes, a phenomenon that is favored for genomes close to or less than 50% of AAV *wild-type* packaging size (Figure S6). While the relative level and contribution in transduction of this dimeric species in the ssAnc80L65 and ssAAV9 is expected to be similar, it was not empirically determined in the current study.

One of the most appealing features of AAV vectors is their ability to transduce non-dividing cells and their excellent neuronal tropism, which make them a tool of choice to study and manipulate brain circuitry or to express therapeutic genes in various neurological contexts.[1,24,25,27–29,31] Often, a strategy by direct intraparenchymal

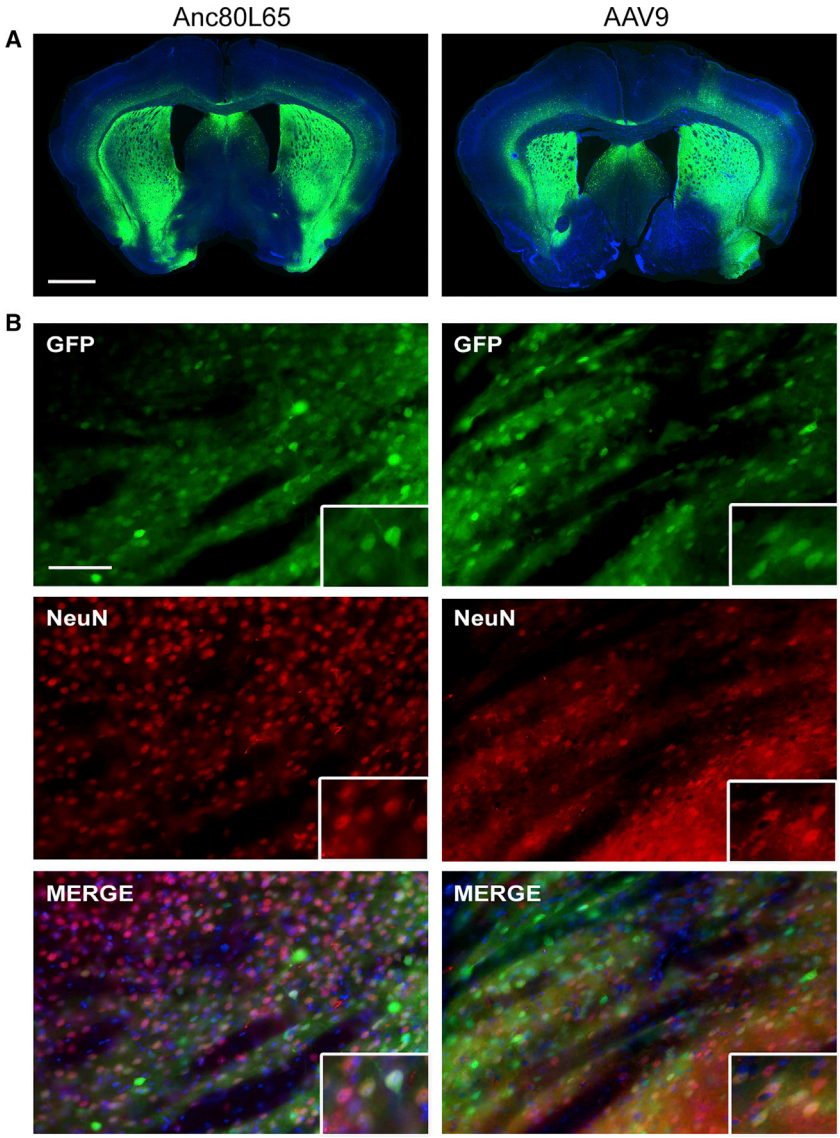

Figure 5. Sustained Neuronal Transduction after Direct Intrastriatal Injection of Anc80L65 and AAV9

(A) Representative images of EGFP fluorescence signal (and DAPI) across the striatum after direct intraparenchymal injection of Anc80L65 or AAV9 (1.5×10^{10} gc/injection site). Scale bar: 1,000 μm. (B) Higher magnification images of the striatum reveal that neurons were mostly transduced with this route of delivery, as demonstrated by the colocalization between EGFP and NeuN. Scale bar: 100 μm.

infusion is chosen to target specific brain regions, and we observed that either direct intraparenchymal or intracerebroventricular injections of Anc80L65 potently transduced neurons and astrocytes in the brain, with similar efficacy as conventional AAV9. Interestingly, i.c.v. delivery of Anc80L65 led to a broader diffusion of the vector than AAV9, extending to the cerebellum. Additionally, a particularly strong tropism for the choroid plexus and the ependymal cells was observed, a feature that may be very valuable for the treatment of specific neurological disorders such as Batten disease[32], spinal muscular atrophy,[68] metachromatic leukodystrophy,[69] mucopolysaccharidosis type IIIA,[70] or Alzheimer's disease.[41] Although strategies by direct intracerebral injection have proven valuable, they still involve moderately invasive surgical procedures that may not become easily translatable to a large number of patients and may not be suitable to impact diffuse neuropathological processes. The discovery that AAV9[47] and several other serotypes (AAVrh.10, AAVrh.39, AAVrh.43, AAV9, and AAV7[46,71]) can cross the blood-brain barrier after systemic infusion and achieve spread transduction of the CNS after minimally invasive surgical procedures has opened novel research avenues in the field of neurosciences. Remarkable benefit has already been demonstrated using i.v. delivery of AAV in multiple animal models,[21,44,72–74] and a first clinical trial has been approved by the FDA to use systemic delivery of AAV9 for the treatment of infantile spinal muscular atrophy type 1.[22] Considering that Anc80L65 is the predicted synthetic ancestor of AAV serotypes 1, 2, 8, and 9, we hypothesized that it may also cross the BBB. Indeed, although the difference in transduction efficacy was minimal after intraparenchymal or intracerebroventricular injections (implying that the steps of receptor-mediated entry, intracellular trafficking, endosomal escape, and intranuclear transport were comparable between Anc80L65 and AAV9), our results demonstrate that peripherally administered Anc80L65 efficiently targets the neural tissue, with an order of magnitude above conventional AAV9. However, the percentages of EGFP-positive cells remained lower when compared with AAV9 harboring an sc genome. The transduction discrepancy between single-stranded and sc AAV administered peripherally has been reported in previous studies,[48,53] an effect potentially related with the rate-limiting conversion of ssDNA to double-stranded genomic DNA, a slow process that relies on host-cell DNA synthesis and delays or impairs transduction.[61,62] By contrast, the increased capacity of Anc80L65 to target the nervous system after peripheral injection as compared with AAV9 necessarily relies on differences of the capsids, which could impact the half-life of the vector within the bloodstream and/or the capacity of the vector to cross vascular endothelial barriers and in particular the BBB. Previous studies have demonstrated that each serotype has a different half-life after systemic infusion, with AAV9 exhibiting a particularly slow blood clearance and sustained infectivity in the bloodstream (up to 24 hr).[75] Additionally, efficient transcytosis of AAV across endothelial cells, which has been demonstrated *in vitro*, could be a determinant factor for CNS gene transfer after peripheral delivery.[76] Indeed,

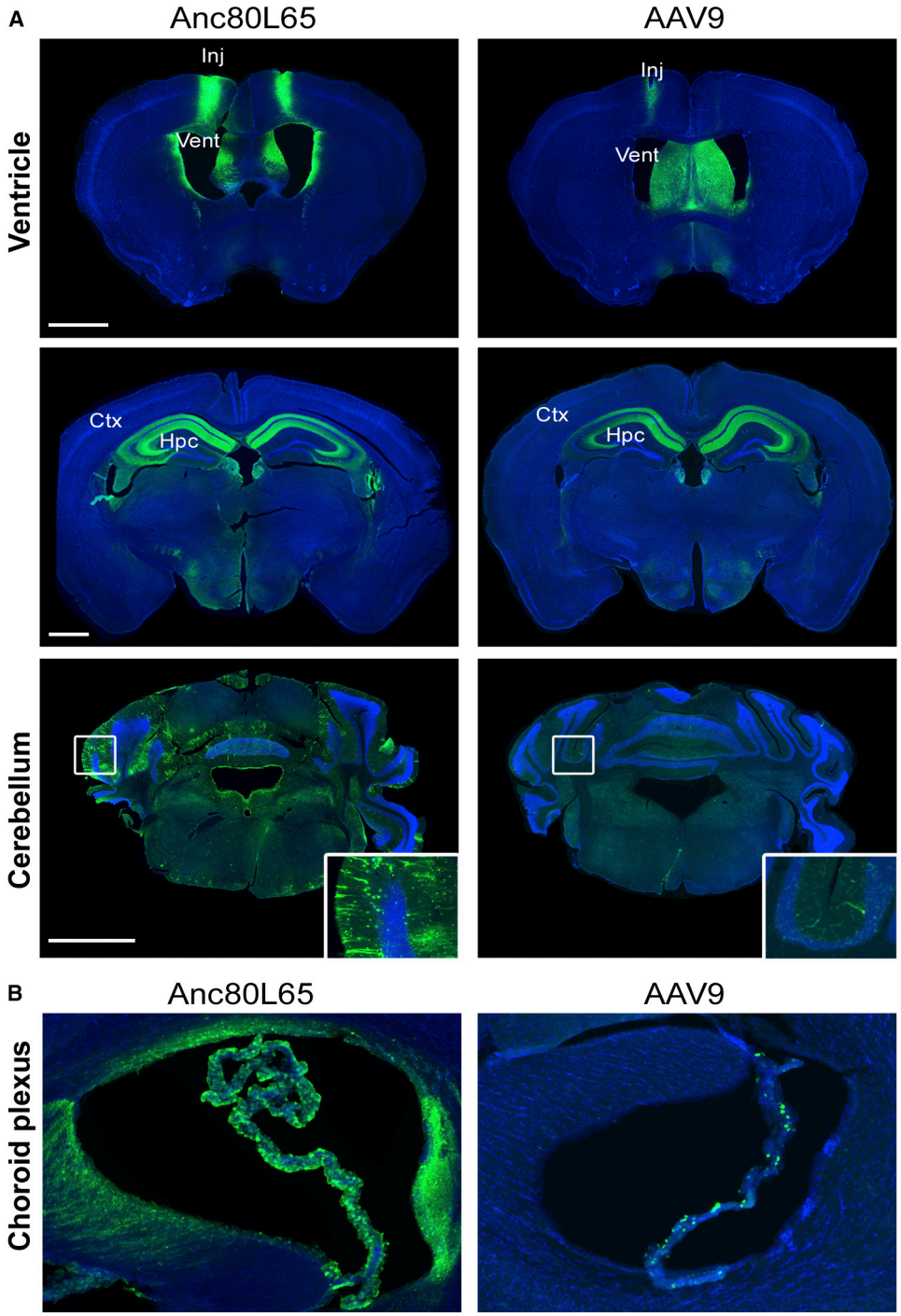

Figure 6. Widespread Diffusion of Anc80L65 as Compared with AAV9 after Intracerebroventricular Injection

(A) Representative images of the EGFP fluorescence intensity detected over three coronal sections after intracerebroventricular infusion of Anc80L65 or AAV9 (4.5×10^{10} gc/injection site). Of interest, although the signal was comparable at the level of the ventricle or in the hippocampus, Anc80L65 appeared to diffuse much more broadly as compared with AAV9, as shown by the increased EGFP fluorescence across the cerebellum. Scale bar: 1,000 μm. (B) Anc80L65 also efficiently targets the choroid plexus, whereas sparse choroid plexus transduction was observed with AAV9.

AAV9 has been shown to shuttle across brain microvascular endothelial cells (BMVECs) more efficiently than AAV2 without compromising the integrity of the BBB. By contrast, AAV2 appears to be directly endocytosed without diffusing through the BMVEC cell layer, resulting in transduction of those cells.[77] Whether those features (blood stability and transcytosis through the BBB) are potentiated with Anc80L65 remains to be determined. In any case, the high efficacy of Anc80L65 harboring a single-stranded genome to transduce the CNS after i.v. infusion makes it a very attractive option for peripheral delivery of a wide variety of genes to the brain and the spinal cord (cloning capacity for a scAAV: ~2.3 kb; for an ssAAV: 4.7kb[78]). Additionally, higher doses of Anc80L65 could be delivered to further increase its transduction efficiency in the nervous system. To date, only a few variants of AAV9 from a library-based selection (AAV-PHP.B, AAV-PHP.eB, and AAV-PHP.S) have been shown to also achieve a high level of transgene expression in the CNS after i.v. administration of recombinant virions carrying a single-stranded genome.[43,45] PHP.B, PHP.eB, and PHP.S, which were not available at the initiation of these studies, are highly potent AAVs that incorporate a peptide in a surface-exposed region of the AAV9 capsid. A library of peptides was successfully selected from a compelling *in vivo* selection strategy in order to identify potent BBB-crossing AAVs, which led to the isolation of AAV.PHP.B and other related variants.[43,45,63,79,80] One concern with orthologous strategies such as the peptide insertion in PHP.B is the risk that a particular technology is active only in the host species it was selected in. Specifically, the inserted peptide may engage a new pathway for transduction as compared with the canonical AAV pathway, which drives the enhanced BBB and CNS biology. Although it is known that the AAV uptake and tropism biology are qualitatively upheld across species (e.g., by the conservation of the AAVR entry receptor), this is not known of these orthologous pathways that AAV normally does not engage, which may impact the ability for vector technologies such as AAVR to translate across species, and eventually to humans. Indeed, a recent study by the group of James M. Wilson[81] demonstrated that AAV.PHP.B's phenotype for enhanced transduction in the CNS following i.v. injection was limited to the C57BL/6 strain in which it was originally derived. By design, Anc80L65 permutates residues on the AAV capsid that were naturally under selective pressure throughout evolution, thereby possibly skewing its transduction biology more toward conserved pathways. Further studies are required, however, to demonstrate whether Anc80L65's findings here do translate to other mouse strains and higher species.

Importantly, although i.v. infusion of Anc80L65 efficiently targeted the brain and spinal cord, very high expression in the liver was also observed (Figures S1 and S2). In fact, at day 3 post-injection, the signal emanating from the liver was 123-fold higher with Anc80L65 than AAV9. This large differential decreased to about 15-fold from day 7 on, due to a slight decrease in expression of Anc80L65 and an increase in expression from days 3 to 7 with AAV9 (Figure S1A). This observation could be partially explained by faster expression kinetics for Anc80L65 versus AAV9, although the mechanism for this is thus far unknown. The decrease of signal between days 3 and 7 in Anc80L65-FLuc-injected mice could be because of transient expression in cells other than hepatocytes (e.g., Kupffer cells, sinusoidal endothelial cells), although future studies will need to address this possibility. The high liver transduction with Anc80L65 raises three concerns when considering translation to the clinic: first, ectopic expression of a foreign protein in an organ that physiologically does not produce it can lead to unpredictable side effects; second, expression of a transgene in the periphery can promote an adverse immune reaction when the protein is initially absent, whereas targeted expression in the neural tissue (referred to as an "immunotolerant" organ) would not lead to such a reaction;[66,82] and third, AAV genotoxicity has occasionally been reported in the liver after infusion of high doses of vector.[83–85] To circumvent those issues and increase the safety of peripherally delivered AAV, strategies to restrict the expression of the transgene specifically in neural cells (using appropriate specific promoters or miRNA)[53,86–88] or to lower Anc80L65 affinity for hepatocytes (approaches known as "liver detargeting"[89]) could be implemented.

Overall, the present study emphasizes the efficacy of ssAnc80L65 as an efficient gene transfer tool to target the CNS after i.v., intracerebroventricular, and i.v. injection. Although those results further investigation of its transduction profile in other species, including non-human primates will warrant its potential as an excellent gene transfer tool.

MATERIALS AND METHODS

AAV Vector Genetic Backbone and Production

A CMV.EGFP.WPRE and CMV.EGFP.T2A.Luciferase.SVPA were cloned into an AAV2 genetic backbone. The expression cassette of the CMV.EGFP.WPRE vector genomes used to produce single-stranded AAV9, Anc80L65, and sc AAV9 (scAAV9) had exactly the same configuration (Figure S6). AAV2/9 and AAV2/Anc80L65 viral stocks were prepared and titered at the Gene Transfer Vector Core (http://vector.meei.harvard.edu) at Massachusetts Eye and Ear. AAV preparations were produced by triple-plasmid transfection as described previously.[90] In brief, large-scale polyethylenimine transfections of AAV *cis*, AAV *trans*, and adenovirus helper plasmid were performed with near-confluent monolayers of HEK293 cells. The downstream purification process was performed following protocols described previously.[90] Viral vectors were resuspended in PBS. DNase I-resistant vector genomes copies were used to titrate AAV preparations by TaqMan qPCR amplification (Applied Biosystems 7500; Life Technologies, Woburn, MA, USA) with primers and probes detecting promoter and transgene of the transgene cassette. The purity was evaluated by SDS-PAGE gel electrophoresis. AAV2/Anc80L65 plasmid reagents are available through http://www.addgene.org/.

Animals and Tail-Vein Injection

All animal experiments were approved by the Institute of Animal Care and Use Committees at the Schepens Eye Research Institute (SERI) and the Massachusetts General Hospital Subcommittee on Research Animal Care following guidelines set forth by the *NIH Guide for the Care and Use of Laboratory Animals*. BALB/c mice or

C57BL/6 females aged 6–8 weeks were purchased from Charles River Laboratories. We used BALB/c mice for *in vivo* bioluminescence imaging because white fur interferes less with the sensitivity of photon detection (compared with black fur). We used C57BL/6 for immunofluorescence detection of EGFP in brain sections because this strain has been used by our laboratory historically for this purpose. For tail-vein injections of AAV vectors, mice were placed into a restrainer (Braintree Scientific, Braintree, MA, USA). The tail was warmed in 40°C water for 30 s before wiping the tail with 70% isopropyl alcohol pads. A 200 μL volume of vector (either 2.0×10^{12} gc/kg for the bioluminescence or 4×10^{13} gc/kg for the EGFP experiments, diluted in PBS) was slowly injected into a lateral tail vein before gently finger-clamping the injection site until bleeding stopped. Animals were euthanized 42 (bioluminescence experiments) or 28 days (immunofluorescence experiments) after injections of Anc80L65/AAV9-Luc or Anc80L65/AAV9-EGFP, respectively. We used a lower dose (5×10^{10} gc/25 g mouse) for the bioluminescence imaging because we were analyzing full-body bioluminescence. At higher AAV doses, the luciferase-induced light emission from the liver is so intense that it can convolute determination of bona fide signal emanating from other body sources.

We used a higher dose (1×10^{12} gc/25 g mouse) in the immunofluorescence experiments, because this is required for detection of EGFP expression in individual cells after i.v. injection.

Stereotactic Intracerebral Injections

Stereotactic intrastriatal and intracerebroventricular injections of AAV9 and Anc80L65 were performed as described previously.[91] Animals were anesthetized by intraperitoneal injection of ketamine/xylazine (100 and 50 mg/kg body weight, respectively) and positioned on a stereotactic frame (Kopf Instruments, Tujunga, CA, USA). Injections of vectors were performed in either the striatum (3 μL of viral suspension/injection site, 1.5×10^{10} gc/mouse) or in the lateral ventricle (5 μL of viral suspension/injection site, 4.5×10^{10} gc/mouse), using a 33G sharp needle attached to a 10-μL Hamilton syringe (Sigma-Aldrich, St. Louis, MO, USA), at a rate of 0.2 μL/min. Stereotactic coordinates of injection sites were calculated from bregma (striatum coordinates: anteroposterior +0.5 mm, mediolateral ±2.5 mm, and dorsoventral −2.5 mm; lateral ventricle coordinates: anteroposterior +0.25 mm, mediolateral ±0.7 mm, and dorsoventral −2 mm).

Immunohistology

Four weeks after injection of Anc80L65, AAV9, and sc AAV9 (scAAV9), mice were given an overdose of anesthesia, transcardially perfused with PBS, and the brain was dissected and post-fixed in 15% glycerol/4% PFA for 48 hr. After cryoprotection in PBS with 30% glycerol for 3 days, 40-μm-thick coronal floating sections were cut using a cryostat microtome for immunohistological analysis. After rinsing off the glycerol in Tris-buffered saline (TBS) buffer, cryosections were permeabilized in 0.5% Triton X-100 (AmericanBio) in TBS for 20 min at room temperature and blocked with 5% normal goat serum (NGS) and 0.5% Triton in TBS for 1 hr at room temperature. Primary antibodies were incubated overnight at 4°C in 2.5% NGS and 0.1% Triton in TBS, whereas Alexa Fluor 488 or Cy3-conjugated secondary antibodies (Jackson Immunoresearch Laboratories, Baltimore, MD, USA) were incubated for 1 hr the next day. Primary antibodies used for this study were chicken anti-GFP (Aves Labs, Tigard, OR, USA), mouse anti-NeuN (EMD Millipore, Burlington, MA, USA), rabbit anti-glutamine synthetase (Abcam, Cambridge, CA, USA), rabbit anti-Olig2 (EMD Millipore, Burlington, MA, USA), rabbit anti-Iba1 (Wako, Japan), rabbit anti-CaMKII (Abcam, Cambridge, MA, USA), mouse anti-GAD67 (EMD Millipore, Burlington, MA, USA), rabbit anti-ChAT (EMD Millipore, Burlington, MA, USA), mouse anti-calbindin (Abcam, Cambridge, MA, USA), rabbit anti-TH (Novus Biologicals, Littleton, CO, USA), and DyLight 594 Lycopersicon Esculentum lectin (Vector Laboratories, Burlingame, CA, USA). Sections were mounted with Vectashield mounting medium with DAPI (Vector Laboratories, Burlingame, CA, USA).

Epifluorescence Microscopy

Tile-scan images were collected on a Zeiss Axio Imager Z epifluorescence microscope equipped with AxioVision software and modified for automated acquisition of entire brain slices, using 5×, 10×, or 20× objectives. Exposure times for each specific immunostaining were set and maintained between each cryosection to preserve consistency.

Stereology-Based Quantitative Analyses

Stereology-based studies were performed as previously described,[92,93] using a motorized stage of an Olympus BX51 epifluorescence microscope equipped with a DP70 digital CCD camera, an X-Cite fluorescent lamp, and the associated CAST stereology software version 2.3.1.5 (Olympus, Tokyo, Japan). The cortex was initially outlined under the 4× objective. Random sampling of the selected area was defined using the optical dissector probe of the CAST software. To evaluate the percentage of Anc80L65, AAV9, and scAAV9 transduced astrocytes or neurons, we performed the stereology-based counts under the 20× objective, with a meander sampling of 10% for the surface of cortex for Anc80L65 and scAAV9, and 30% for AAV9 (the EGFP-positive cells being seldom in this case). For each counting frame, the total number of astrocytes (GS-positive cells) or neurons (NeuN-positive cells) was evaluated, and among each of those populations, the percentages of EGFP-positive cells. Only glial and neuronal cells with a DAPI-positive nucleus within the counting frame were considered. Counts were performed blindly.

Tissue DNA Biodistribution

Snap-frozen tissue was proteinase K digested, and genomic DNA (gDNA) was extracted using the Blood & Cell Culture DNA Mini kit (Qiagen, Germantown, MD, USA) as indicated. Isolated gDNA was quantified using the BioTek plate reading spectrophotometer (BioTek Instruments, Winooski, VT, USA). gc distribution in diploid cells were detected and quantified by qPCR using Applied Biosystems 7500 Real-Time PCR Systems with TaqMan PCR master mix reagents (Applied Biosystems, Woburn, MA, USA) and transgene-specific primer/probes.

Bioluminescence Imaging

Imaging experiments were performed using the IVIS Spectrum imager outfitted with an XGI-8 gas anesthesia system (PerkinElmer, Waltham, MA, USA). Mice were anesthetized and then injected intraperitoneally with 4.5 mg of D-luciferin substrate (Sigma-Aldrich, St. Louis, MO, USA) resuspended in 150 μL of PBS. Five minutes post-substrate injection, mice were imaged for luciferase expression using auto-acquisition. We acquired bioluminescence using the auto-exposure setting. Quantitative analysis of bioluminescence images was performed using Living Image software (Perkin Elmer). Regions of interest were carefully circumscribed around each body area (e.g., liver, head), and the light emission expressed in photons per second in graphical format. In bioluminescence images, the scale is depicted as radiance (photons/s/cm^2/steradian).

Statistics

Statistical analysis of data was performed using GraphPad Prism software (version 5.01). Because of the small number of animals per experimental group, the normality test was not conclusive (D'Agostino-Pearson normality test). A non-parametric one-way ANOVA test (Kruskal-Wallis test) followed by a Dunn's multiple comparisons test was therefore performed. A p value <0.05 was considered to be statistically significant. For statistical analysis of bioluminescence assays, comparison between two groups was performed using an unpaired t test. Data are represented as the mean with SD.

SUPPLEMENTAL INFORMATION

Supplemental Information includes six figures and can be found with this article online at https://doi.org/10.1016/j.omtm.2018.07.006.

AUTHOR CONTRIBUTIONS

L.H.V., E.H., C.A.M., E.A.-M., and B.T.H. designed the study, interpreted the results, and wrote the manuscript. E.H., C.A.M., E.A.-M., E.P.L., A.V., and O.C. performed the experiments.

CONFLICTS OF INTEREST

L.H.V. is an inventor of AAV-Anc and other AAV technologies, which are licensed to various biotechnology and pharmaceutical entities.

ACKNOWLEDGMENTS

This work was supported by NIH/NIA grant 1K99AG047336-01A1 (to E.H.). C.M. received support from the American Brain Tumor Association and the Cure Alzheimer's Fund. L.H.V. was supported by NIH, National Eye Institute Core grant P30EY003790, Giving/Grousbeck, and Lonza Houston.

REFERENCES

1. Choudhury, S.R., Hudry, E., Maguire, C.A., Sena-Esteves, M., Breakefield, X.O., and Grandi, P. (2017). Viral vectors for therapy of neurologic diseases. Neuropharmacology *120*, 63–80.

2. Zinn, E., and Vandenberghe, L.H. (2014). Adeno-associated virus: fit to serve. Curr. Opin. Virol. *8*, 90–97.

3. McCarty, D.M., Young, S.M., Jr., and Samulski, R.J. (2004). Integration of adeno-associated virus (AAV) and recombinant AAV vectors. Annu. Rev. Genet. *38*, 819–845.

4. Bessis, N., GarciaCozar, F.J., and Boissier, M.C. (2004). Immune responses to gene therapy vectors: influence on vector function and effector mechanisms. Gene Ther. *11* (*Suppl 1*), S10–S17.

5. Leone, P., Shera, D., McPhee, S.W., Francis, J.S., Kolodny, E.H., Bilaniuk, L.T., Wang, D.J., Assadi, M., Goldfarb, O., Goldman, H.W., et al. (2012). Long-term follow-up after gene therapy for canavan disease. Sci. Transl. Med. *4*, 165ra163.

6. Chamberlain, J.R., and Chamberlain, J.S. (2017). Progress toward Gene Therapy for Duchenne Muscular Dystrophy. Mol. Ther. *25*, 1125–1131.

7. Ajufo, E., and Cuchel, M. (2016). Recent Developments in Gene Therapy for Homozygous Familial Hypercholesterolemia. Curr. Atheroscler. Rep. *18*, 22.

8. Koo, T., Popplewell, L., Athanasopoulos, T., and Dickson, G. (2014). Triple trans-splicing adeno-associated virus vectors capable of transferring the coding sequence for full-length dystrophin protein into dystrophic mice. Hum. Gene Ther. *25*, 98–108.

9. Mak, K.Y., Rajapaksha, I.G., Angus, P.W., and Herath, C.B. (2017). The adeno-associated virus - a safe and effective vehicle for liver-specific gene therapy of inherited and non-inherited diseases. Curr. Gene Ther. *17*, 4–16.

10. Chamberlain, K., Riyad, J.M., and Weber, T. (2017). Cardiac gene therapy with adeno-associated virus-based vectors. Curr. Opin. Cardiol. *32*, 275–282.

11. Craig, A.J., and Housley, G.D. (2016). Evaluation of gene therapy as an intervention strategy to treat brain injury from stroke. Front. Mol. Neurosci. *9*, 34.

12. Beutler, A.S., and Reinhardt, M. (2009). AAV for pain: steps towards clinical translation. Gene Ther. *16*, 461–469.

13. Park, K., Kim, W.J., Cho, Y.H., Lee, Y.I., Lee, H., Jeong, S., Cho, E.S., Chang, S.I., Moon, S.K., Kang, B.S., et al. (2008). Cancer gene therapy using adeno-associated virus vectors. Front. Biosci. *13*, 2653–2659.

14. Limberis, M.P., Adam, V.S., Wong, G., Gren, J., Kobasa, D., Ross, T.M., Kobinger, G.P., Tretiakova, A., and Wilson, J.M. (2013). Intranasal antibody gene transfer in mice and ferrets elicits broad protection against pandemic influenza. Sci. Transl. Med. *5*, 187ra72.

15. Balazs, A.B., Bloom, J.D., Hong, C.M., Rao, D.S., and Baltimore, D. (2013). Broad protection against influenza infection by vectored immunoprophylaxis in mice. Nat. Biotechnol. *31*, 647–652.

16. Balazs, A.B., Chen, J., Hong, C.M., Rao, D.S., Yang, L., and Baltimore, D. (2011). Antibody-based protection against HIV infection by vectored immunoprophylaxis. Nature *481*, 81–84.

17. Johnson, P.R., Schnepp, B.C., Zhang, J., Connell, M.J., Greene, S.M., Yuste, E., Desrosiers, R.C., and Clark, K.R. (2009). Vector-mediated gene transfer engenders long-lived neutralizing activity and protection against SIV infection in monkeys. Nat. Med. *15*, 901–906.

18. Nathwani, A.C., Reiss, U.M., Tuddenham, E.G., Rosales, C., Chowdary, P., McIntosh, J., Della Peruta, M., Lheriteau, E., Patel, N., Raj, D., et al. (2014). Long-term safety and efficacy of factor IX gene therapy in hemophilia B. N. Engl. J. Med. *371*, 1994–2004.

19. George, L.A., Sullivan, S.K., Giermasz, A., Rasko, J.E.J., Samelson-Jones, B.J., Ducore, J., Cuker, A., Sullivan, L.M., Majumdar, S., Teitel, J., et al. (2017). Hemophilia B gene therapy with a high-specific-activity Factor IX variant. N. Engl. J. Med. *377*, 2215–2227.

20. Rangarajan, S., Walsh, L., Lester, W., Perry, D., Madan, B., Laffan, M., Yu, H., Vettermann, C., Pierce, G.F., Wong, W.Y., and Pasi, K.J. (2017). AAV5-factor VIII gene transfer in severe hemophilia A. N. Engl. J. Med. *377*, 2519–2530.

21. Meyer, K., Ferraiuolo, L., Schmelzer, L., Braun, L., McGovern, V., Likhite, S., Michels, O., Govoni, A., Fitzgerald, J., Morales, P., et al. (2015). Improving single injection CSF delivery of AAV9-mediated gene therapy for SMA: a dose-response study in mice and nonhuman primates. Mol. Ther. *23*, 477–487.

22. Mendell, J.R., Al-Zaidy, S., Shell, R., Arnold, W.D., Rodino-Klapac, L.R., Prior, T.W., Lowes, L., Alfano, L., Berry, K., Church, K., et al. (2017). Single-dose gene-replacement therapy for spinal muscular atrophy. N. Engl. J. Med. *377*, 1713–1722.

23. Russell, S., Bennett, J., Wellman, J.A., Chung, D.C., Yu, Z.F., Tillman, A., Wittes, J., Pappas, J., Elci, O., McCague, S., et al. (2017). Efficacy and safety of voretigene

neparvovec (AAV2-hRPE65v2) in patients with RPE65-mediated inherited retinal dystrophy: a randomised, controlled, open-label, phase 3 trial. Lancet *390*, 849–860.

24. Gaj, T., Epstein, B.E., and Schaffer, D.V. (2016). Genome engineering using adeno-associated virus: basic and clinical research applications. Mol. Ther. *24*, 458–464.
25. Swiech, L., Heidenreich, M., Banerjee, A., Habib, N., Li, Y., Trombetta, J., Sur, M., and Zhang, F. (2015). In vivo interrogation of gene function in the mammalian brain using CRISPR-Cas9. Nat. Biotechnol. *33*, 102–106.
26. Tang, W., Szokol, K., Jensen, V., Enger, R., Trivedi, C.A., Hvalby, Ø., Helm, P.J., Looger, L.L., Sprengel, R., and Nagelhus, E.A. (2015). Stimulation-evoked Ca2+ signals in astrocytic processes at hippocampal CA3-CA1 synapses of adult mice are modulated by glutamate and ATP. J. Neurosci. *35*, 3016–3021.
27. Ekstrand, M.I., Nectow, A.R., Knight, Z.A., Latcha, K.N., Pomeranz, L.E., and Friedman, J.M. (2014). Molecular profiling of neurons based on connectivity. Cell *157*, 1230–1242.
28. Xu, W., and Südhof, T.C. (2013). A neural circuit for memory specificity and generalization. Science *339*, 1290–1295.
29. Cai, D., Cohen, K.B., Luo, T., Lichtman, J.W., and Sanes, J.R. (2013). Improved tools for the Brainbow toolbox. Nat. Methods *10*, 540–547.
30. Shimano, T., Fyk-Kolodziej, B., Mirza, N., Asako, M., Tomoda, K., Bledsoe, S., Pan, Z.H., Molitor, S., and Holt, A.G. (2013). Assessment of the AAV-mediated expression of channelrhodopsin-2 and halorhodopsin in brainstem neurons mediating auditory signaling. Brain Res. *1511*, 138–152.
31. Kaspar, B.K., Vissel, B., Bengoechea, T., Crone, S., Randolph-Moore, L., Muller, R., Brandon, E.P., Schaffer, D., Verma, I.M., Lee, K.F., et al. (2002). Adeno-associated virus effectively mediates conditional gene modification in the brain. Proc. Natl. Acad. Sci. USA *99*, 2320–2325.
32. Katz, M.L., Tecedor, L., Chen, Y., Williamson, B.G., Lysenko, E., Wininger, F.A., Young, W.M., Johnson, G.C., Whiting, R.E., Coates, J.R., and Davidson, B.L. (2015). AAV gene transfer delays disease onset in a TPP1-deficient canine model of the late infantile form of Batten disease. Sci. Transl. Med. *7*, 313ra180.
33. Sargeant, T.J., Wang, S., Bradley, J., Smith, N.J., Raha, A.A., McNair, R., Ziegler, R.J., Cheng, S.H., Cox, T.M., and Cachón-González, M.B. (2011). Adeno-associated virus-mediated expression of β-hexosaminidase prevents neuronal loss in the Sandhoff mouse brain. Hum. Mol. Genet. *20*, 4371–4380.
34. Sevin, C., Benraiss, A., Van Dam, D., Bonnin, D., Nagels, G., Verot, L., Laurendeau, I., Vidaud, M., Gieselmann, V., Vanier, M., et al. (2006). Intracerebral adeno-associated virus-mediated gene transfer in rapidly progressive forms of metachromatic leukodystrophy. Hum. Mol. Genet. *15*, 53–64.
35. Passini, M.A., Macauley, S.L., Huff, M.R., Taksir, T.V., Bu, J., Wu, I.H., Piepenhagen, P.A., Dodge, J.C., Shihabuddin, L.S., O'Riordan, C.R., et al. (2005). AAV vector-mediated correction of brain pathology in a mouse model of Niemann-Pick A disease. Mol. Ther. *11*, 754–762.
36. Gelfand, Y., and Kaplitt, M.G. (2013). Gene therapy for psychiatric disorders. World Neurosurg. *80*, S32.e11–18.
37. Chen, G., Twyman, R., and Manji, H.K. (2010). p11 and gene therapy for severe psychiatric disorders: a practical goal? Sci. Transl. Med. *2*, 54ps51.
38. Liu, W., Zhao, L., Blackman, B., Parmar, M., Wong, M.Y., Woo, T., Yu, F., Chiuchiolo, M.J., Sondhi, D., Kaminsky, S.M., et al. (2016). Vectored intracerebral immunization with the anti-tau monoclonal antibody PHF1 markedly reduces tau pathology in mutant tau transgenic mice. J. Neurosci. *36*, 12425–12435.
39. Zharikov, A.D., Cannon, J.R., Tapias, V., Bai, Q., Horowitz, M.P., Shah, V., El Ayadi, A., Hastings, T.G., Greenamyre, J.T., and Burton, E.A. (2015). shRNA targeting α-synuclein prevents neurodegeneration in a Parkinson's disease model. J. Clin. Invest. *125*, 2721–2735.
40. Foust, K.D., Salazar, D.L., Likhite, S., Ferraiuolo, L., Ditsworth, D., Ilieva, H., Meyer, K., Schmelzer, L., Braun, L., Cleveland, D.W., and Kaspar, B.K. (2013). Therapeutic AAV9-mediated suppression of mutant SOD1 slows disease progression and extends survival in models of inherited ALS. Mol. Ther. *21*, 2148–2159.
41. Hudry, E., Dashkoff, J., Roe, A.D., Takeda, S., Koffie, R.M., Hashimoto, T., Scheel, M., Spires-Jones, T., Arbel-Ornath, M., Betensky, R., et al. (2013). Gene transfer of human Apoe isoforms results in differential modulation of amyloid deposition and neurotoxicity in mouse brain. Sci. Transl. Med. *5*, 212ra161.
42. Hester, M.E., Foust, K.D., Kaspar, R.W., and Kaspar, B.K. (2009). AAV as a gene transfer vector for the treatment of neurological disorders: novel treatment thoughts for ALS. Curr. Gene Ther. *9*, 428–433.
43. Chan, K.Y., Jang, M.J., Yoo, B.B., Greenbaum, A., Ravi, N., Wu, W.L., Sánchez-Guardado, L., Lois, C., Mazmanian, S.K., Deverman, B.E., and Gradinaru, V. (2017). Engineered AAVs for efficient noninvasive gene delivery to the central and peripheral nervous systems. Nat. Neurosci. *20*, 1172–1179.
44. Choudhury, S.R., Harris, A.F., Cabral, D.J., Keeler, A.M., Sapp, E., Ferreira, J.S., Gray-Edwards, H.L., Johnson, J.A., Johnson, A.K., Su, Q., et al. (2016). Widespread central nervous system gene transfer and silencing after systemic delivery of novel AAV-AS vector. Mol. Ther. *24*, 726–735.
45. Deverman, B.E., Pravdo, P.L., Simpson, B.P., Kumar, S.R., Chan, K.Y., Banerjee, A., Wu, W.L., Yang, B., Huber, N., Pasca, S.P., and Gradinaru, V. (2016). Cre-dependent selection yields AAV variants for widespread gene transfer to the adult brain. Nat. Biotechnol. *34*, 204–209.
46. Yang, B., Li, S., Wang, H., Guo, Y., Gessler, D.J., Cao, C., Su, Q., Kramer, J., Zhong, L., Ahmed, S.S., et al. (2014). Global CNS transduction of adult mice by intravenously delivered rAAVrh.8 and rAAVrh.10 and nonhuman primates by rAAVrh.10. Mol. Ther. *22*, 1299–1309.
47. Foust, K.D., Nurre, E., Montgomery, C.L., Hernandez, A., Chan, C.M., and Kaspar, B.K. (2009). Intravascular AAV9 preferentially targets neonatal neurons and adult astrocytes. Nat. Biotechnol. *27*, 59–65.
48. Gray, S.J., Matagne, V., Bachaboina, L., Yadav, S., Ojeda, S.R., and Samulski, R.J. (2011). Preclinical differences of intravascular AAV9 delivery to neurons and glia: a comparative study of adult mice and nonhuman primates. Mol. Ther. *19*, 1058–1069.
49. Fu, H., Dirosario, J., Killedar, S., Zaraspe, K., and McCarty, D.M. (2011). Correction of neurological disease of mucopolysaccharidosis IIIB in adult mice by rAAV9 trans-blood-brain barrier gene delivery. Mol. Ther. *19*, 1025–1033.
50. Bevan, A.K., Duque, S., Foust, K.D., Morales, P.R., Braun, L., Schmelzer, L., Chan, C.M., McCrate, M., Chicoine, L.G., Coley, B.D., et al. (2011). Systemic gene delivery in large species for targeting spinal cord, brain, and peripheral tissues for pediatric disorders. Mol. Ther. *19*, 1971–1980.
51. Duque, S., Joussemet, B., Riviere, C., Marais, T., Dubreil, L., Douar, A.M., Fyfe, J., Moullier, P., Colle, M.A., and Barkats, M. (2009). Intravenous administration of self-complementary AAV9 enables transgene delivery to adult motor neurons. Mol. Ther. *17*, 1187–1196.
52. Samaranch, L., Salegio, E.A., San Sebastian, W., Kells, A.P., Foust, K.D., Bringas, J.R., Lamarre, C., Forsayeth, J., Kaspar, B.K., and Bankiewicz, K.S. (2012). Adeno-associated virus serotype 9 transduction in the central nervous system of nonhuman primates. Hum. Gene Ther. *23*, 382–389.
53. Dashkoff, J., Lerner, E.P., Truong, N., Klickstein, J.A., Fan, Z., Mu, D., Maguire, C.A., Hyman, B.T., and Hudry, E. (2016). Tailored transgene expression to specific cell types in the central nervous system after peripheral injection with AAV9. Mol. Ther. Methods Clin. Dev. *3*, 16081.
54. de Leeuw, C.N., Dyka, F.M., Boye, S.L., Laprise, S., Zhou, M., Chou, A.Y., Borretta, L., McInerny, S.C., Banks, K.G., Portales-Casamar, E., et al. (2014). Targeted CNS delivery using human MiniPromoters and demonstrated compatibility with adeno-associated viral vectors. Mol. Ther. Methods Clin. Dev. *1*, 5.
55. Zinn, E., Pacouret, S., Khaychuk, V., Turunen, H.T., Carvalho, L.S., Andres-Mateos, E., Shah, S., Shelke, R., Maurer, A.C., Plovie, E., et al. (2015). In silico reconstruction of the viral evolutionary lineage yields a potent gene therapy vector. Cell Rep. *12*, 1056–1068.
56. Wang, L., Xiao, R., Andres-Mateos, E., and Vandenberghe, L.H. (2017). Single stranded adeno-associated virus achieves efficient gene transfer to anterior segment in the mouse eye. PLoS ONE *12*, e0182473.
57. Carvalho, L.S., Xiao, R., Wassmer, S.J., Langsdorf, A., Zinn, E., Pacouret, S., Shah, S., Comander, J.I., Kim, L.A., Lim, L., and Vandenberghe, L.H. (2018). Synthetic adeno-associated viral vector efficiently targets mouse and nonhuman primate retina in vivo. Hum. Gene Ther. Published online March 20, 2018. https://doi.org/10.1089/hum.2017.154.
58. Landegger, L.D., Pan, B., Askew, C., Wassmer, S.J., Gluck, S.D., Galvin, A., Taylor, R., Forge, A., Stankovic, K.M., Holt, J.R., and Vandenberghe, L.H. (2017). A synthetic

AAV vector enables safe and efficient gene transfer to the mammalian inner ear. Nat. Biotechnol. *35*, 280–284.

59. Pan, B., Askew, C., Galvin, A., Heman-Ackah, S., Asai, Y., Indzhykulian, A.A., Jodelka, F.M., Hastings, M.L., Lentz, J.J., Vandenberghe, L.H., et al. (2017). Gene therapy restores auditory and vestibular function in a mouse model of Usher syndrome type 1c. Nat. Biotechnol. *35*, 264–272.

60. Suzuki, J., Hashimoto, K., Xiao, R., Vandenberghe, L.H., and Liberman, M.C. (2017). Cochlear gene therapy with ancestral AAV in adult mice: complete transduction of inner hair cells without cochlear dysfunction. Sci. Rep. *7*, 45524.

61. McCarty, D.M. (2008). Self-complementary AAV vectors; advances and applications. Mol. Ther. *16*, 1648–1656.

62. Wang, Z., Ma, H.I., Li, J., Sun, L., Zhang, J., and Xiao, X. (2003). Rapid and highly efficient transduction by double-stranded adeno-associated virus vectors in vitro and in vivo. Gene Ther. *10*, 2105–2111.

63. Davidsson, M., Diaz-Fernandez, P., Schwich, O.D., Torroba, M., Wang, G., and Björklund, T. (2016). A novel process of viral vector barcoding and library preparation enables high-diversity library generation and recombination-free paired-end sequencing. Sci. Rep. *6*, 37563.

64. Gao, G., Vandenberghe, L.H., and Wilson, J.M. (2005). New recombinant serotypes of AAV vectors. Curr. Gene Ther. *5*, 285–297.

65. Gao, G.P., Alvira, M.R., Wang, L., Calcedo, R., Johnston, J., and Wilson, J.M. (2002). Novel adeno-associated viruses from rhesus monkeys as vectors for human gene therapy. Proc. Natl. Acad. Sci. USA *99*, 11854–11859.

66. Mingozzi, F., and High, K.A. (2013). Immune responses to AAV vectors: overcoming barriers to successful gene therapy. Blood *122*, 23–36.

67. Calcedo, R., Vandenberghe, L.H., Gao, G., Lin, J., and Wilson, J.M. (2009). Worldwide epidemiology of neutralizing antibodies to adeno-associated viruses. J. Infect. Dis. *199*, 381–390.

68. Armbruster, N., Lattanzi, A., Jeavons, M., Van Wittenberghe, L., Gjata, B., Marais, T., Martin, S., Vignaud, A., Voit, T., Mavilio, F., et al. (2016). Efficacy and biodistribution analysis of intracerebroventricular administration of an optimized scAAV9-SMN1 vector in a mouse model of spinal muscular atrophy. Mol. Ther. Methods Clin. Dev. *3*, 16060.

69. Hironaka, K., Yamazaki, Y., Hirai, Y., Yamamoto, M., Miyake, N., Miyake, K., Okada, T., Morita, A., and Shimada, T. (2015). Enzyme replacement in the CSF to treat metachromatic leukodystrophy in mouse model using single intracerebroventricular injection of self-complementary AAV1 vector. Sci. Rep. *5*, 13104.

70. Haurigot, V., Marcó, S., Ribera, A., Garcia, M., Ruzo, A., Villacampa, P., Ayuso, E., Añor, S., Andaluz, A., Pineda, M., et al. (2013). Whole body correction of mucopolysaccharidosis IIIA by intracerebrospinal fluid gene therapy. J. Clin. Invest. *123*, 3254–3271.

71. Zhang, H., Yang, B., Mu, X., Ahmed, S.S., Su, Q., He, R., Wang, H., Mueller, C., Sena-Esteves, M., Brown, R., et al. (2011). Several rAAV vectors efficiently cross the blood-brain barrier and transduce neurons and astrocytes in the neonatal mouse central nervous system. Mol. Ther. *19*, 1440–1448.

72. Bosch, M.E., Aldrich, A., Fallet, R., Odvody, J., Burkovetskaya, M., Schuberth, K., Fitzgerald, J.A., Foust, K.D., and Kielian, T. (2016). Self-complementary AAV9 gene delivery partially corrects pathology associated with juvenile neuronal ceroid lipofuscinosis (CLN3). J. Neurosci. *36*, 9669–9682.

73. Crommentuijn, M.H., Kantar, R., Noske, D.P., Vandertop, W.P., Badr, C.E., Würdinger, T., Maguire, C.A., and Tannous, B.A. (2016). Systemically administered AAV9-sTRAIL combats invasive glioblastoma in a patient-derived orthotopic xenograft model. Mol. Ther. Oncolytics *3*, 16017.

74. Gong, Y., Mu, D., Prabhakar, S., Moser, A., Musolino, P., Ren, J., Breakefield, X.O., Maguire, C.A., and Eichler, F.S. (2015). Adenoassociated virus serotype 9-mediated gene therapy for x-linked adrenoleukodystrophy. Mol. Ther. *23*, 824–834.

75. Kotchey, N.M., Adachi, K., Zahid, M., Inagaki, K., Charan, R., Parker, R.S., and Nakai, H. (2011). A potential role of distinctively delayed blood clearance of recombinant adeno-associated virus serotype 9 in robust cardiac transduction. Mol. Ther. *19*, 1079–1089.

76. Di Pasquale, G., and Chiorini, J.A. (2006). AAV transcytosis through barrier epithelia and endothelium. Mol. Ther. *13*, 506–516.

77. Merkel, S.F., Andrews, A.M., Lutton, E.M., Mu, D., Hudry, E., Hyman, B.T., Maguire, C.A., and Ramirez, S.H. (2017). Trafficking of adeno-associated virus vectors across a model of the blood-brain barrier; a comparative study of transcytosis and transduction using primary human brain endothelial cells. J. Neurochem. *140*, 216–230.

78. Wu, J., Zhao, W., Zhong, L., Han, Z., Li, B., Ma, W., Weigel-Kelley, K.A., Warrington, K.H., and Srivastava, A. (2007). Self-complementary recombinant adeno-associated viral vectors: packaging capacity and the role of rep proteins in vector purity. Hum. Gene Ther. *18*, 171–182.

79. Ojala, D.S., Sun, S., Santiago-Ortiz, J.L., Shapiro, M.G., Romero, P.A., and Schaffer, D.V. (2018). In vivo selection of a computationally designed SCHEMA AAV library yields a novel variant for infection of adult neural stem cells in the SVZ. Mol Ther *26*, 304–319.

80. Choudhury, S.R., Fitzpatrick, Z., Harris, A.F., Maitland, S.A., Ferreira, J.S., Zhang, Y., Ma, S., Sharma, R.B., Gray-Edwards, H.L., Johnson, J.A., et al. (2016). In vivo selection yields AAV-B1 capsid for central nervous system and muscle gene therapy. Mol. Ther. *24*, 1247–1257.

81. Hordeaux, J., Wang, Q., Katz, N., Buza, E.L., Bell, P., and Wilson, J.M. (2018). The neurotropic properties of AAV-PHP.B are limited to C57BL/6J mice. Mol. Ther. *26*, 664–668.

82. Zaiss, A.K., and Muruve, D.A. (2005). Immune responses to adeno-associated virus vectors. Curr. Gene Ther. *5*, 323–331.

83. Nault, J.C., Datta, S., Imbeaud, S., Franconi, A., Mallet, M., Couchy, G., Letouzé, E., Pilati, C., Verret, B., Blanc, J.F., et al. (2015). Recurrent AAV2-related insertional mutagenesis in human hepatocellular carcinomas. Nat. Genet. *47*, 1187–1193.

84. Rosas, L.E., Grieves, J.L., Zaraspe, K., La Perle, K.M., Fu, H., and McCarty, D.M. (2012). Patterns of scAAV vector insertion associated with oncogenic events in a mouse model for genotoxicity. Mol. Ther. *20*, 2098–2110.

85. Li, H., Malani, N., Hamilton, S.R., Schlachterman, A., Bussadori, G., Edmonson, S.E., Shah, R., Arruda, V.R., Mingozzi, F., Wright, J.F., et al. (2011). Assessing the potential for AAV vector genotoxicity in a murine model. Blood *117*, 3311–3319.

86. Kügler, S. (2016). Tissue-specific promoters in the CNS. Methods Mol. Biol. *1382*, 81–91.

87. Mudannayake, J.M., Mouravlev, A., Fong, D.M., and Young, D. (2016). Transcriptional activity of novel ALDH1L1 promoters in the rat brain following AAV vector-mediated gene transfer. Mol. Ther. Methods Clin. Dev. *3*, 16075.

88. Malmevik, J., Petri, R., Klussendorf, T., Knauff, P., Åkerblom, M., Johansson, J., Soneji, S., and Jakobsson, J. (2015). Identification of the miRNA targetome in hippocampal neurons using RIP-seq. Sci. Rep. *5*, 12609.

89. Pulicherla, N., Shen, S., Yadav, S., Debbink, K., Govindasamy, L., Agbandje-McKenna, M., and Asokan, A. (2011). Engineering liver-detargeted AAV9 vectors for cardiac and musculoskeletal gene transfer. Mol. Ther. *19*, 1070–1078.

90. Lock, M., Alvira, M., Vandenberghe, L.H., Samanta, A., Toelen, J., Debyser, Z., and Wilson, J.M. (2010). Rapid, simple, and versatile manufacturing of recombinant adeno-associated viral vectors at scale. Hum. Gene Ther. *21*, 1259–1271.

91. Hudry, E., Van Dam, D., Kulik, W., De Deyn, P.P., Stet, F.S., Ahouansou, O., Benraiss, A., Delacourte, A., Bougnères, P., Aubourg, P., and Cartier, N. (2010). Adeno-associated virus gene therapy with cholesterol 24-hydroxylase reduces the amyloid pathology before or after the onset of amyloid plaques in mouse models of Alzheimer's disease. Mol. Ther. *18*, 44–53.

92. Hudry, E., Martin, C., Gandhi, S., György, B., Scheffer, D.I., Mu, D., Merkel, S.F., Mingozzi, F., Fitzpatrick, Z., Dimant, H., et al. (2016). Exosome-associated AAV vector as a robust and convenient neuroscience tool. Gene Ther. *23*, 380–392.

93. Serrano-Pozo, A., Muzikansky, A., Gómez-Isla, T., Growdon, J.H., Betensky, R.A., Frosch, M.P., and Hyman, B.T. (2013). Differential relationships of reactive astrocytes and microglia to fibrillar amyloid deposits in Alzheimer disease. J. Neuropathol. Exp. Neurol. *72*, 462–471.

OMTM, Volume *10*

Supplemental Information

Efficient Gene Transfer to the Central Nervous System by Single-Stranded Anc80L65

Eloise Hudry, Eva Andres-Mateos, Eli P. Lerner, Adrienn Volak, Olivia Cohen, Bradley T. Hyman, Casey A. Maguire, and Luk H. Vandenberghe

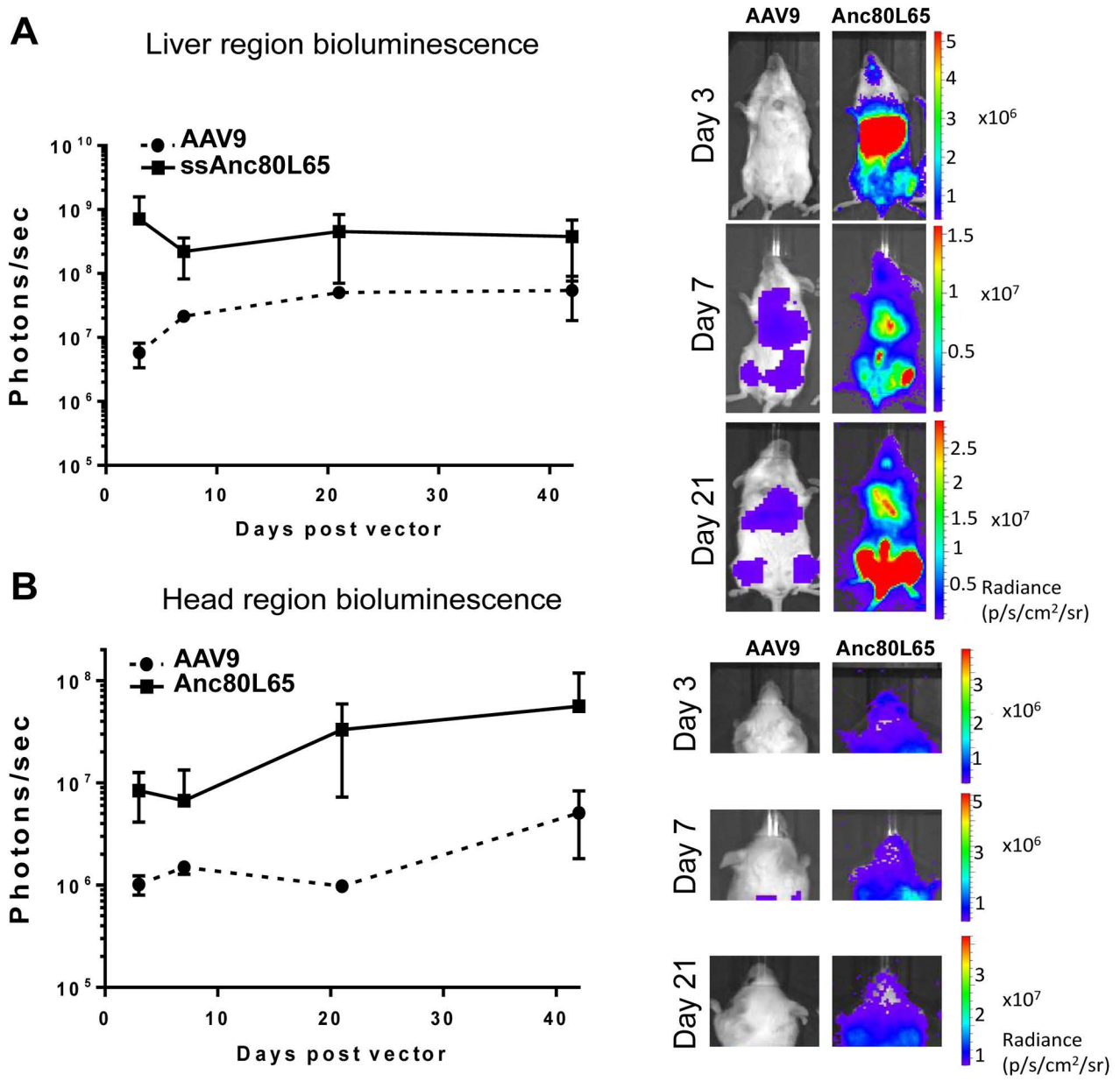
A
Liver region bioluminescence
AAV9
ssAnc80L65
Photons/sec
Days post vector
B
Head region bioluminescence
AAV9
Anc80L65
Photons/sec
Days post vector
AAV9
Anc80L65
Day 3
Day 7
Day 21
x10^6
x10^7
Radiance (p/s/cm²/sr)

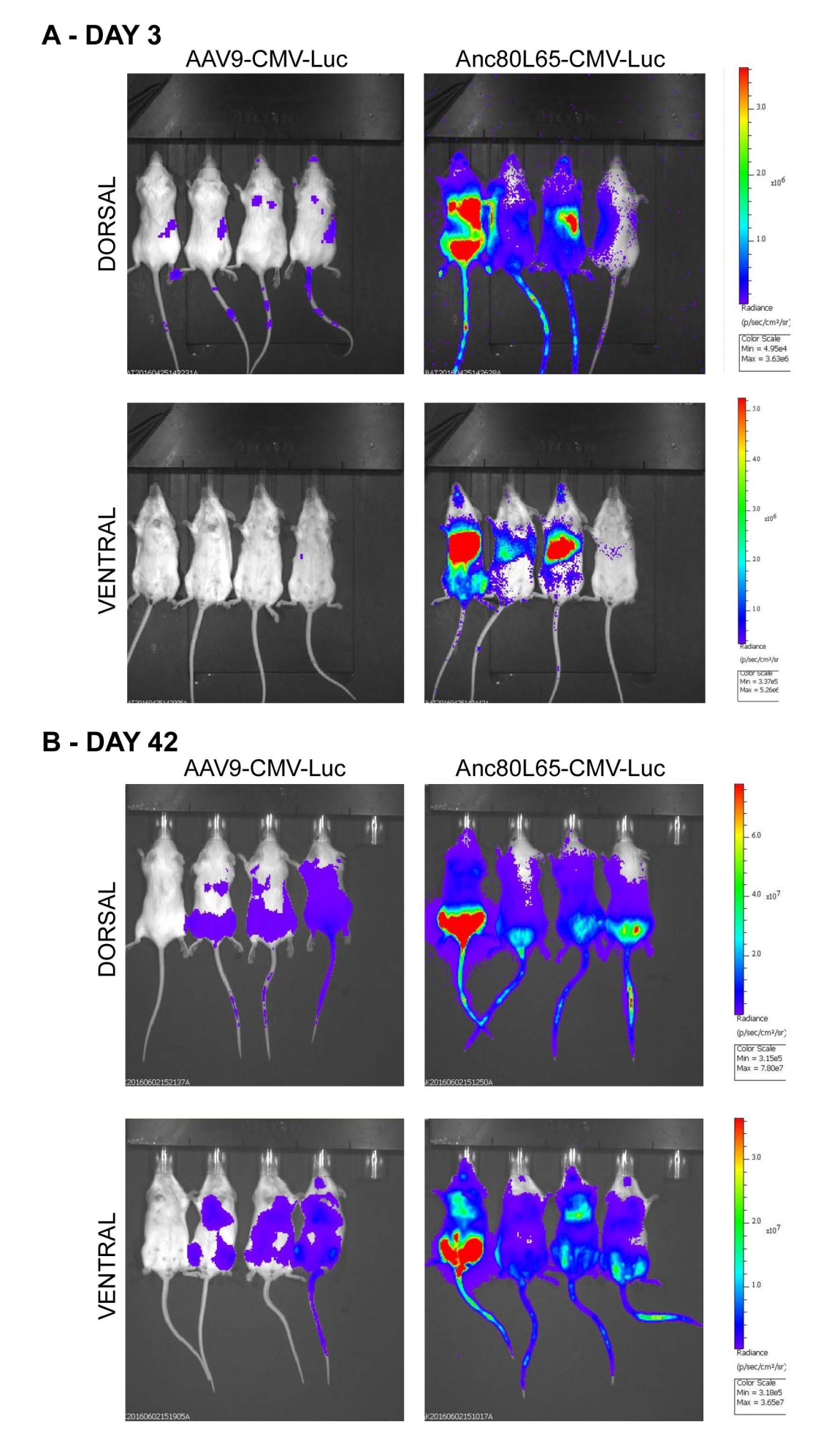
A - DAY 3
AAV9-CMV-Luc
Anc80L65-CMV-Luc
DORSAL
VENTRAL
3.0
2.0
x10^6
1.0
Radiance
(p/sec/cm²/sr)
Color Scale
Min = 4.95e4
Max = 3.63e6
5.0
4.0
3.0
x10^6
2.0
1.0
Radiance
(p/sec/cm²/sr
Color Scale
Min = 3.37e5
Max = 5.26e6
B - DAY 42
AAV9-CMV-Luc
Anc80L65-CMV-Luc
DORSAL
VENTRAL
6.0
4.0
x10^7
2.0
Radiance
(p/sec/cm²/sr)
Color Scale
Min = 3.15e5
Max = 7.80e7
3.0
2.0
x10^7
1.0
Radiance
(p/sec/cm²/sr)
Color Scale
Min = 3.18e5
Max = 3.65e7

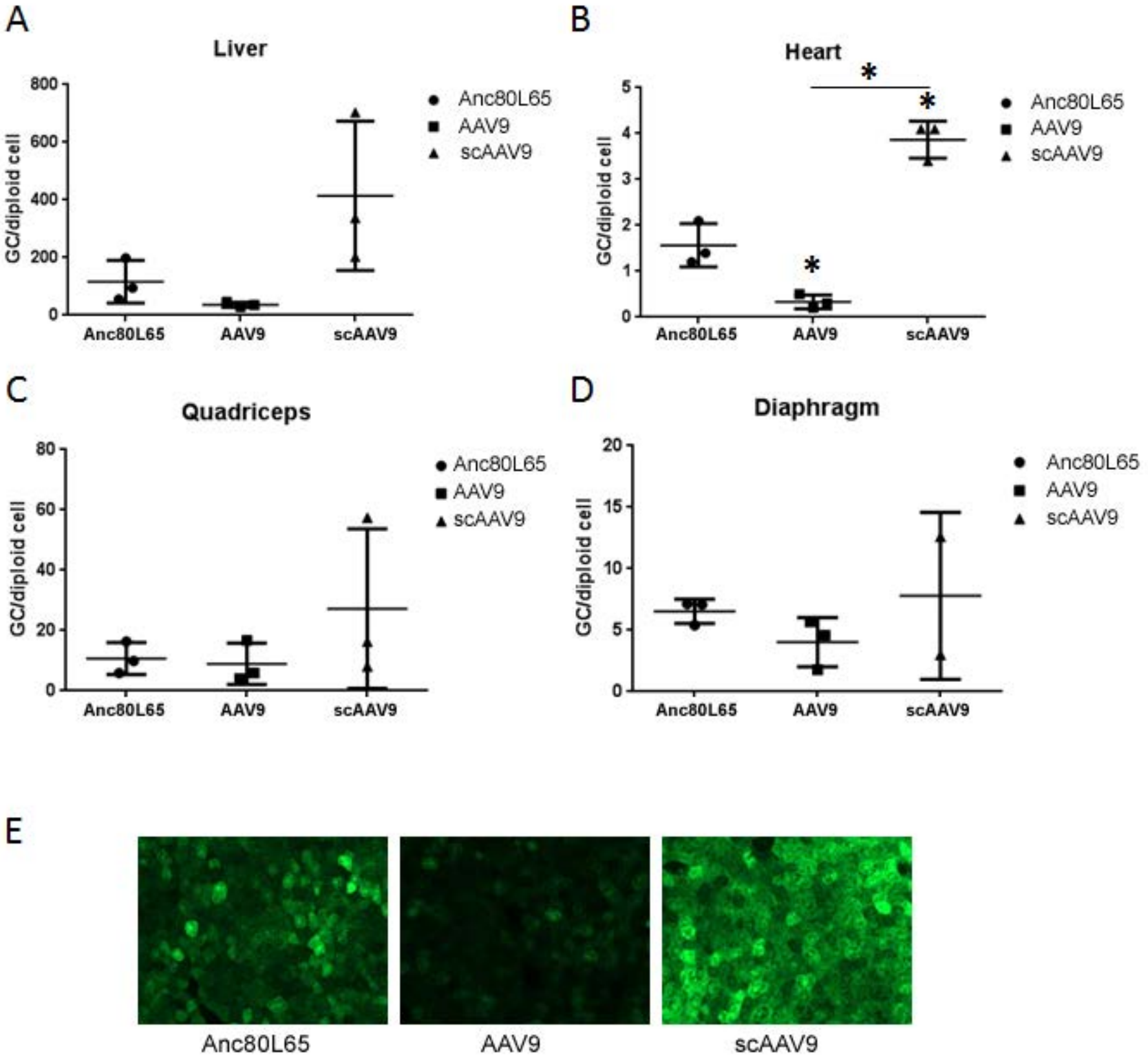
A
Liver
GC/diploid cell
800
600
400
200
0
Anc80L65
AAV9
scAAV9
B
Heart
GC/diploid cell
5
4
3
2
1
0
*
*
*
Anc80L65
AAV9
scAAV9
C
Quadriceps
GC/diploid cell
80
60
40
20
0
Anc80L65
AAV9
scAAV9
D
Diaphragm
GC/diploid cell
20
15
10
5
0
Anc80L65
AAV9
scAAV9
E
Anc80L65
AAV9
scAAV9

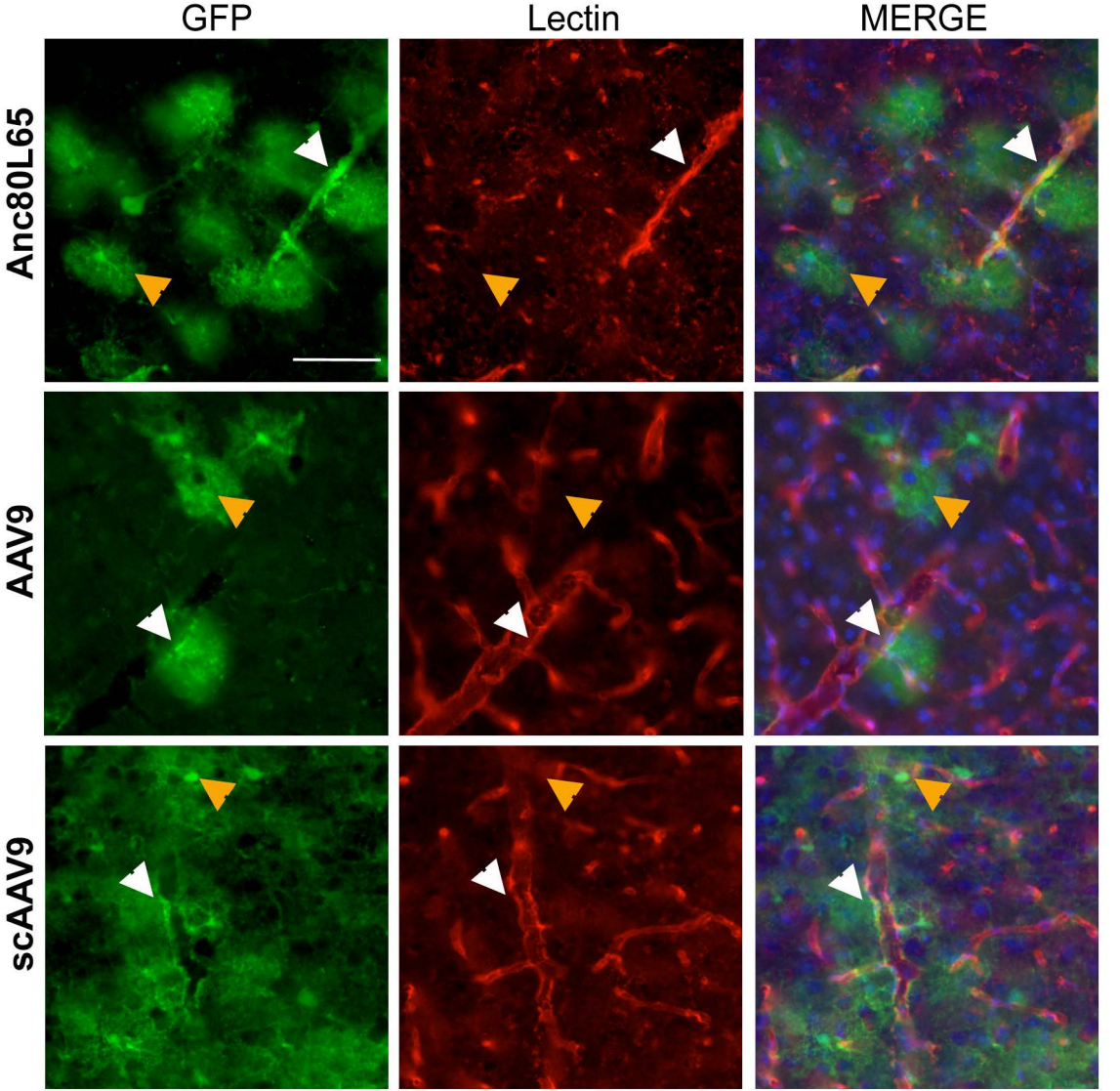
GFP
Lectin
MERGE
Anc80L65
AAV9
scAAV9

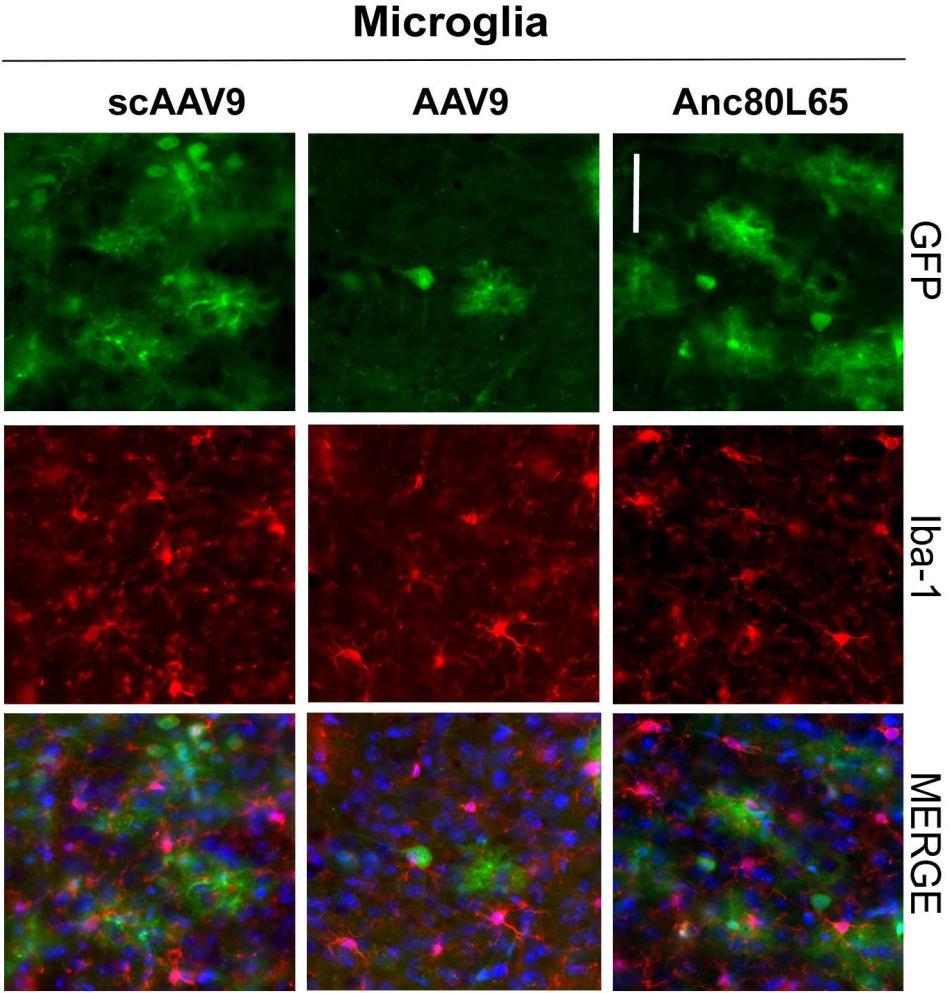
Microglia
scAAV9
AAV9
Anc80L65
GFP
Iba-1
MERGE

A

Bioluminescence

B

Systemic and intracerebral injection

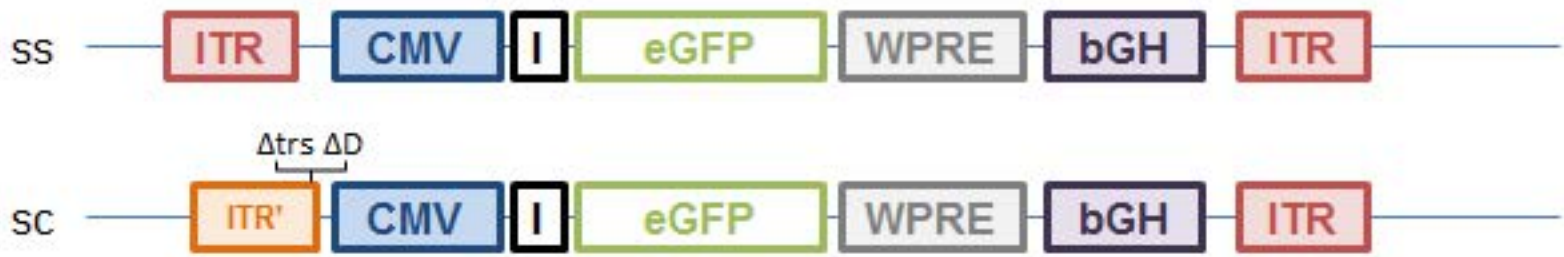

C

VECTOR	DOSE	ROUTE OF ADMINISTRATION
BIOLUMINESCENCE		
AAV2/9.CMV.EGFP.T2A.LUCIFERASE.SVPA	2E12 gc/kg	Intravenous
AAV2/Anc80.CMV.EGFP.T2A.LUCIFERASE.SVPA	2E12 gc/kg	Intravenous
SYSTEMIC INJECTION		
AAV2/9.CMV.EGFP.WPRE.bGH	4E13 gc/kg	Intravenous
AAV2/Anc80.CMV.EGFP.WPRE.bGH	4E13 gc/kg	Intravenous
SC AAV2/9.CMV.EGFP.WPRE.bGH	4E13 gc/kg	Intravenous
INTRACEREBRAL INJECTION		
AAV2/9.CMV.EGFP.WPRE.bGH	1.5E10 gc/mouse	Intra-striatal
AAV2/Anc80.CMV.EGFP.WPRE.bGH	1.5E10 gc/mouse	Intra-striatal
AAV2/9.CMV.EGFP.WPRE.bGH	4.5E10 gc/mouse	Intra-ventricular
AAV2/Anc80.CMV.EGFP.WPRE.bGH	4.5E10 gc/mouse	Intra-ventricular

SUPPLEMENTAL FIGURES LEGENDS

Supplementary Figure 1. Kinetics and localization of bioluminescence signal after intravenous injection of BALB/c with Anc80L65-CMV-FLuc or AAV9-CMV-FLuc.
Mice were injected with $2x10^{12}$ gc/kg of vector and imaged at days 3, 7, 21, and 42 post injection. (A) Bioluminescence signal from liver region. A region of interest (ROI) was drawn on each image and photons/sec calculated. Left: graph depicting kinetics of expression. Right: representative images of mice injected with AAV9 or Anc80 at days 3, 7, and 21 post injection. (B) Bioluminescence signal from head region. ROI was drawn on each image and photons/sec calculated. Left: graph depicting kinetics of expression. Right: representative images of mice injected with AAV9 or Anc80L65 at days 3, 7, and 21 post injection. n=5 mice/group.

Supplementary Figure 2. Whole-body bioluminescence images at days 3 and 42 post intravenous injection of Anc80L65-CMV-FLuc or AAV9-CMV-FLuc
Representative bioluminescence images of BALB/c mice injected systemically with $2x10^{12}$ gc/kg of AAV9-CMV-FLuc or Anc80-CMV-FLuc, at 3 and 42 days after injection in the lateral tail vein.

Supplementary Figure 3. Quantification of AAV genome-copy numbers in peripheral tissues after systemic injection with Anc80L65-CMV-eGFP, AAV9-CMV-eGFP and scAAV9-CMV-eGFP
Genomic DNA qPCR analysis was performed to measure the gc/diploid cell in liver (A), heart (B), quadriceps (C) and diaphragm (D), n=3 mice per group; two-way ANOVA followed by Tukey's multiple comparison test; *$p<0.05$. (E) Representative images of eGFP fluorescence signal detected across the liver after intravenous injection of the same dose of Anc80L65, AAV9 and scAAV9 in wild-type mice ($4x10^{13}$gc/kg).

Supplementary Figure 4. Anc80L65, AAV9 and scAAV9 transduction of intraparenchymal and vessel-associated astrocytes
Double immunostaining with Lycopersicon Esculentum lectin ("Lectin") and eGFP shows that both astrocytic endfeet and parenchymal astrocytes were equivalently transduced by Anc80L65, AAV9 or scAAV9 after systemic infusion. Scale bar: 50µm

Supplementary Figure 5. Absence of microglial transduction after intravenous delivery of Anc80L65, AAV9 and scAAV9 harboring a self-complementary genome
Double immunostaining with Iba-1 and eGFP was performed in order to determine if Anc80L65, AAV9 or AAV9 containing a self-complementary genome (scAAV9) transduced microglial cells. As shown on those representative images, no colocalization between the two markers was detected. Scale bar: 50µm

Supplementary Figure 6. Vector and experimental design
(A and B) Schematic representation of the expression cassette used to produce the viral vectors. (A) For the bioluminescence experiments a multicistronic vector with a T2A peptide signal was used. A 133 base pairs chimeric intron (I) and the viral SV40 polyA signal (SVPA) were introduced in the cassette. (B) For the systemic and intracerebral injection, the self-complementary (sc) vector 5' ITR contained a deletion of the D-sequence and the terminal resolution site mutation (trs). The transgene design (CMV.eGFP.WPRE.bGH, 2266 base pairs) was identical for the self-complementary and single stranded vectors, and included a 133 bp chimeric intron (I) and the bovine growth hormone polyA signal (bGH). (C) Table including the vector, dose and route of administration used in all the experiments.